Structure and emission studies of Schiff-base [2+2] macrocycles derived from 2,2′-oxydianiline and the ROP capability of their organoaluminium complexes.

Wenxue Yang,[a] Ke-Qing Zhao,[a] Timothy J. Prior,[b] David L. Hughes,[c] Abdessamad Arbaoui,[c] Tiezheng Bian,[c] Yimin Chao,[c] Mark R.J. Elsegood [d] and Carl Redshaw [a,b*]

[a] *College of Chemistry and Materials Science, Sichuan Normal University, Chengdu, 610066, China.*

[b] *Department of Chemistry, University of Hull, Hull, HU6 7RX, U.K.*

[c] *School of Chemistry, University of East Anglia, Norwich, NR4 7TJ, U.K.*

[d] *Chemistry Department, Loughborough University, Loughborough, Leicestershire, LE11 3TU, U.K.*

Abstract: The molecular structures of a number of solvates of the [2+2] Schiff-base macrocycles {[2-(OH)-5-(R)-C_6H_2-1,3-$(CH)_2$][O(2-$C_6H_4N)_2$]}$_2$ (R = Me $\mathbf{L^1}H_2$, *t*Bu $\mathbf{L^2}H_2$, Cl $\mathbf{L^3}H_2$), formed by reacting 2,6-dicarboxy-4-R-phenol with 2,2′-oxydianiline (2-aminophenylether), $(2\text{-}NH_2C_6H_4)_2O$, have been have been determined. Their emission properties have been investigated: $\mathbf{L^3}H_2$ exhibited a hypochromic shift of the macrocycle emission in different solvents, from λ_{max} at 508 nm (in acetonitrile) to 585 nm (in dichloromethane). Reaction of $\mathbf{L^n}H_2$ with two equivalents of AlR'_3 (R′ = Me, Et) afforded dinuclear alkylaluminium complexes [$(AlR'_2)_2L^{1\text{-}3}$] (R = R′ = Me (**1**), R = *t*Bu, R′ = Me (**2**), R = Cl, R′ = Me (**3**), R = Me, R′ = Et (**4**), R = *t*Bu, R′ = Et (**5**), R = Cl, R′ = Et (**6**)). For comparative studies, reactions of two equivalents of AlR'_3 (R′ = Me, Et) with the macrocycle derived from 2,2′-ethylenedianiline and 2,6-dicarboxy-R-phenols (R = Me $\mathbf{L^4}H_2$, *t*Bu $\mathbf{L^5}H_2$) were conducted; the complexes [(AlMe)$(AlMe_2)\mathbf{L^5}$]·$2^1/_4$MeCN (**7**·$2^1/_4$MeCN) and [$(AlEt_2)_2\mathbf{L^4}$] (**8**) were isolated. Use of

limited $AlEt_3$ with $\mathbf{L^3}H_2$ or $\mathbf{L^5}H_2$ afforded mononuclear bis(macrocyclic) complexes [Al($\mathbf{L^3}$)($\mathbf{L^3}$H)]·4toluene (**9**·4toluene) and [Al($\mathbf{L^5}$)($\mathbf{L^5}$H)]·5MeCN (**10**·5MeCN), respectively. Use of four equivalents of AlR'_3 led to transfer of alkyl groups and isolation of the complexes [$(AlR'_2)_4\mathbf{L^{1'-3'}}$] (R = $\mathbf{L^{2'}}$, R′ = Me (**11**); $\mathbf{L^{3'}}$, R′ = Me (**12**); $\mathbf{L^{1'}}$, R′ = Et (**13**); $\mathbf{L^{2'}}$, R′ = Et (**14**); $\mathbf{L^{3'}}$, R′ = Et (**15**)), where $\mathbf{L^{1'-3'}}$ is the macrocycle resulting from double alkyl transfer to imine, namely {[2-(O)-5-(R)C_6H_2-1-(CH)-3-(C(R′)H][(O)(2-(N)-2′-$C_6H_4N)_2$]}$_2$. Molecular structures of complexes **7**·2$^1/_4$MeCN, **8**, **9**·4toluene, **10**·5MeCN and **11**·1¾toluene·1$^1/_4$hexane are reported. These complexes act as catalysts for the ring opening polymerisation (ROP) of ε-caprolactone and *rac*-lactide; high conversions were achieved over 30 mins at 80 ^oC for ε-caprolactone, and 110 ^oC over 12 h for *rac*-lactide.

Keywords: Schiff-base; macrocycle; structures; solvents; emission; organoaluminium; ring opening polymerisation.

Introduction

Fluorescent organic materials are attracting current interest in areas such as opto-electronics and cellular imaging. [1] Organic materials usually give bright emission set at a specific wavelength, although certain materials exhibit solvatochromism, which is the change in the optical properties of a material upon a change of the solvent polarity. A good example is *trans*-4-dimethylamino-4′-(1-oxybutyl)stilbene (DOS), which exhibits solvatochromism across the entire visible spectrum with shifts of hundreds of nanometers. [2] Whilst solvatochromic materials have potential applications in bio- and environmental sensing, such applications (molecular recognition and ion sensing) are well established in macrocyclic chemistry. [3] Combining solvatochromism with the inherent molecular recognition

properties of macrocycles, opens up the possibility of intriguing bimodal sensing possibilities. Given that Schiff-base compounds have attracted attention over the years primarily for their biological activity, [4] macrocyclic Schiff bases are of potential interest given their multiple binding sites. [5] We have been investigating the simplest members of this Schiff-base macrocyclic family, so-called Robson type macrocycles, derived from the [2+2] condensation of a diamine with a dialdehyde, specifically herein 1,3-diformylphenol in combination with the diamine 2,2′-oxydianiline, 2-(2-aminophenoxy)aniline, $(2\text{-}NH_2C_6H_4)_2O$. The structural chemistry of this particular macrocycle is unexplored, indeed a search of the CSD revealed no hits, [6a] other than our recently reported manganese chemistry. [6b] Our interest stems primarily from their coordination chemistry and the potential to bind multiple metal centres in close proximity, [6, 7] particular those which could be of use for ring opening polymerisation (ROP) of cyclic esters to produce biodegradable polymers. [8] Poly(ε-caprolactone), PCL, and poly(lactide), PLA, are favoured polymers given both their biodegradability, and that their co-polymers are considered as potential environmentally friendly commodity plastic. [9] Given the central role played by metal complex induced coordination/insertion type ROP processes, investigations into new combinations of metals and ancillary ligands are pivotal when trying to identify structure-activity relationships. Indeed, in previous work, [7a] we communicated how remote alkylaluminium centres bound to a Schiff-base macrocycle derived from the dianiline $[(CH_2CH_2)(2\text{-}C_6H_4NH_2)_2]$ exhibited beneficial cooperative effects in the ROP of ε-caprolactone, whereas the presence of aluminoxane type (Al–O–Al) bonding proved detrimental. Given this, we have re-focused our efforts on such Schiff-base systems and have extended our studies to [2+2] macrocycles derived from the dianiline $(2\text{-}NH_2C_6H_4)_2O$ (see chart 1). Herein, we report the molecular structures of a number of these [2+2] macrocycles, and find that they tend to adopt a taco-like, folded conformation. Investigation of their emission properties in various solvents reveals some interesting solvatochromism

for the macrocyclic system, the emission from which can be tuned by *ca* 77 nm. Interestingly, a series of zinc complexes bearing phenol compartmental type ligation were recently found to exhibit controllable photophysical properties by manipulation of the substituent (Me, *t*Bu, Cl) positioned *para* to the phenolic group. [10]

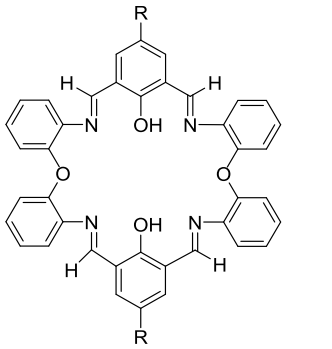

$\mathbf{L}^{1\text{-}3}H_2$; R=Me, *t*Bu, Cl

Chart 2. [2+2] Schiff-base macrocycles of type $\mathbf{L}^{1\text{-}3}H_2$.

Furthermore, we have investigated the reaction chemistry of $\mathbf{L}^{1\text{-}3}H_2$ towards the alkylaluminium reagents R_3Al (R = Me, Et) and have isolated some unexpected products (chart 3). Given this, related studies on macrocycles derived from the ethylene-bridged dianiline $[(CH_2CH_2)(2\text{-}C_6H_4NH_2)_2]$ were conducted, and the ability of these complexes to act as catalysts for the ring opening polymerisation (ROP) of ε-caprolactone and *rac*-lactide has been investigated. The use of alkylaluminium complexes for the ROP of cyclic esters has recently been reviewed. [11]

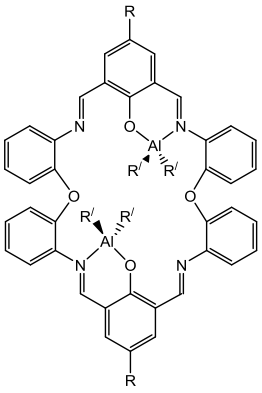

R = R′ = Me (**1**)
R = *t*Bu, R′ = Me (**2**)
R = Cl, R′ = Me (**3**)
R = Me, R′ = Et (**4**)
R = *t*Bu, R′ = Et (**5**)
R = Cl, R′ = Et (**6**)

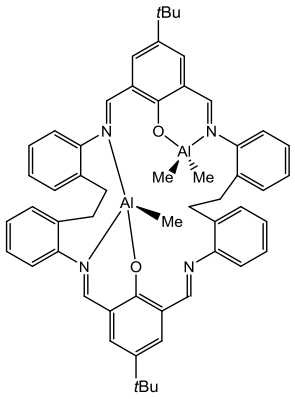

7

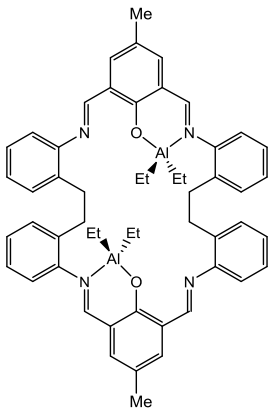

8

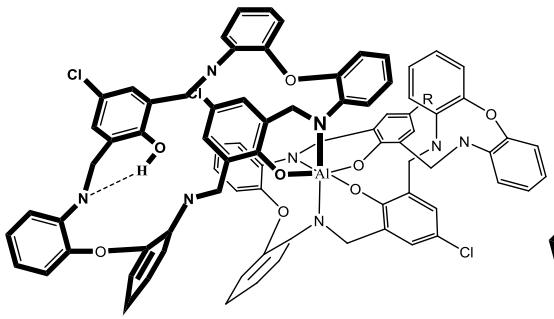

9

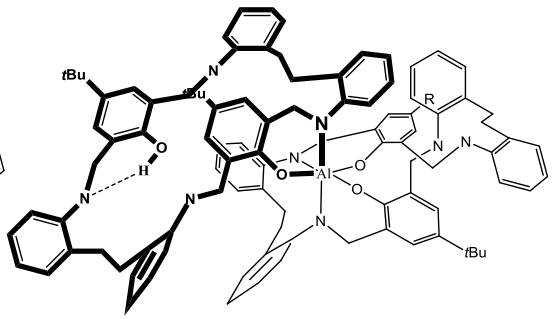

10

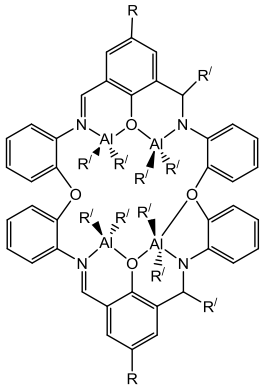

R = Me, R′ = Me (**11**)
R = Cl, R′ = Me (**12**)
R = Me, R′ = Et (**13**)
R = Cl, R′ = Et (**14**)

Chart 3. Aluminium complexes **1 - 14** prepared herein.

Results and Discussion

Preparation, structure and emission studies on $\boldsymbol{L^nH_2}$

The [2+2] Schiff base macrocycles of type $\mathbf{L^nH_2}$ are readily available in high yield *via* the reaction of 2,6-dicarboxy-4-R-phenol, where R = Me (n = 1) , *t*Bu (n = 2) or Cl (n = 3), with 2,2′-oxydianiline, $(2\text{-}NH_2C_6H_4)_2O$. In the IR spectra, *ν*(C=N) for $\mathbf{L^1H_2}$ (1626 cm^{-1}), $\mathbf{L^2H_2}$ (1630 cm^{-1}) and $\mathbf{L^3H_2}$ (1627 cm^{-1})

bands are strong and are very similar to those reported for related ethylene (-CH_2CH_2-) bridged bis(imino)phenoxide macrocycles (1627 – 1629 cm^{-1}), [6b, 7] and also lie within the range reported for other Schiff-base macrocycles. [12] In the ^{1}H NMR spectra, the imino hydrogen chemical shifts for $\mathbf{L^2}H_2$ (8.40 ppm) and $\mathbf{L^3}H_2$ (8.43 ppm) are comparable with those reported previously for bis(imino)phenol-based macrocycles [8.12 to 8.66 ppm] [13], whilst that for $\mathbf{L^1}H_2$ (8.87 ppm) is shifted slightly downfield.

These condensation products {[2-(OH)-5-(R)C_6H_2-1,3-$(CH)_2$][(O)(2-$C_6H_4N)_2$]}$_2$ (R = Me $\mathbf{L^1}H_2$, *t*Bu $\mathbf{L^2}H_2$, Cl $\mathbf{L^3}H_2$) can be recrystallized from a variety of solvents; the molecular structures of a number of solvates are described below. Selected bond lengths and angles for each of the solvates are either discussed in the text or, in the case of $\mathbf{L^2}H_2$, are presented in Table 1, with crystallographic parameters for all structures collated in Table 5. In each case, crystals of $\mathbf{L^n}H_2$ suitable for an X-ray diffraction study were grown from the respective solvent on prolonged standing at ambient temperature. The molecular structure of $\mathbf{L^1}H_2$·MeCN is shown in Figure 1. In the asymmetric unit, there is one macrocycle and one molecule of MeCN. The macrocycle adopts an open, taco-like conformation, and the orientation of the two sides of the macrocycle can be monitored by looking at the cleft angle ϕ (ϕ is defined as the angle subtended between the mean planes of the two phenolate rings (O1 C1-C6, C8, C42, N1, N4 and C21-C27, C29, N2, N3, O3) as illustrated in Figure 2). Thus, the smaller the cleft angle, the more parallel are the sides and the more taco-like the conformation. In the case of $\mathbf{L^1}H_2$·MeCN, the open-taco description reflects the approximate cleft angle of 89.2 ^{o}. A more detailed analysis of the orientation of the rings is presented in Table S1 (see ESI). The MeCN molecule is encapsulated by the macrocycle between the rings incorporating C(19) and C(43). The centroid-to-centroid distance is approximately 8.5 Å, whilst the shortest $H_{(MeCN)}$ to centroid distances are 3.76 and 3.66 Å. The closest neighbour of the MeCN methyl group is the phenolic group with O(1)···H(52c) at

2.51 Å. The compound displays strong intramolecular hydrogen bonds involving the phenolic hydrogen and an imino nitrogen [H(1)···N(1) = 1.74(3) Å and H(3)···N(3) = 1.59(3) Å; O(1)–H(1)···N(1) = 150(3) ^{o} and O(3)–H(3)···N(3) = 152(3) ^{o}].

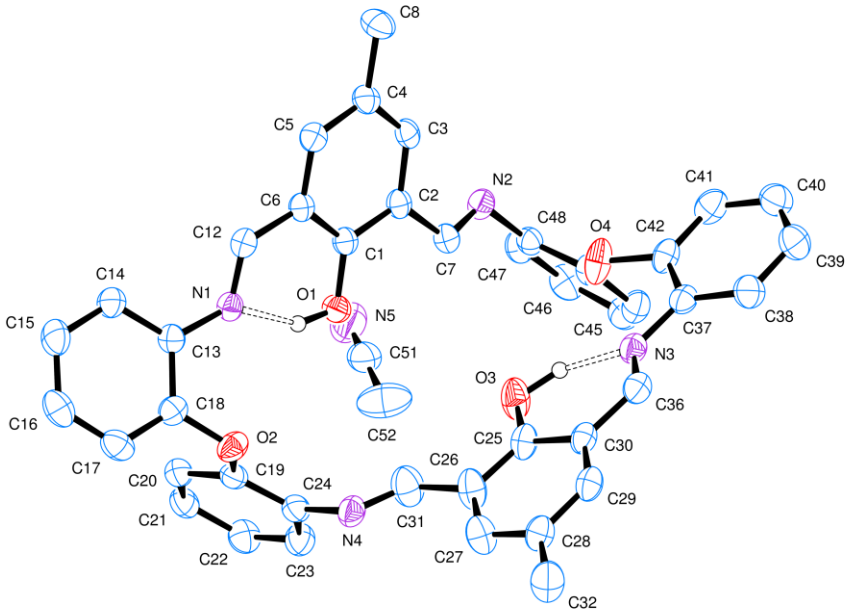

Figure 1. Molecular structure of $\mathbf{L^1}H_2$·MeCN. Selected bond lengths (Å) and angles (^{o}): N(1) – C(12) 1.284(2), N(1) – C(13) 1.415(2), N(2) – C(7) 1.276(2), N(2) – C(48) 1.419(2); C(6) – C(12) – N(1) 121.50(13), C(2) – C(7) – N(2) 121.44(14). H atoms not involved in H-bonding are omitted for clarity.

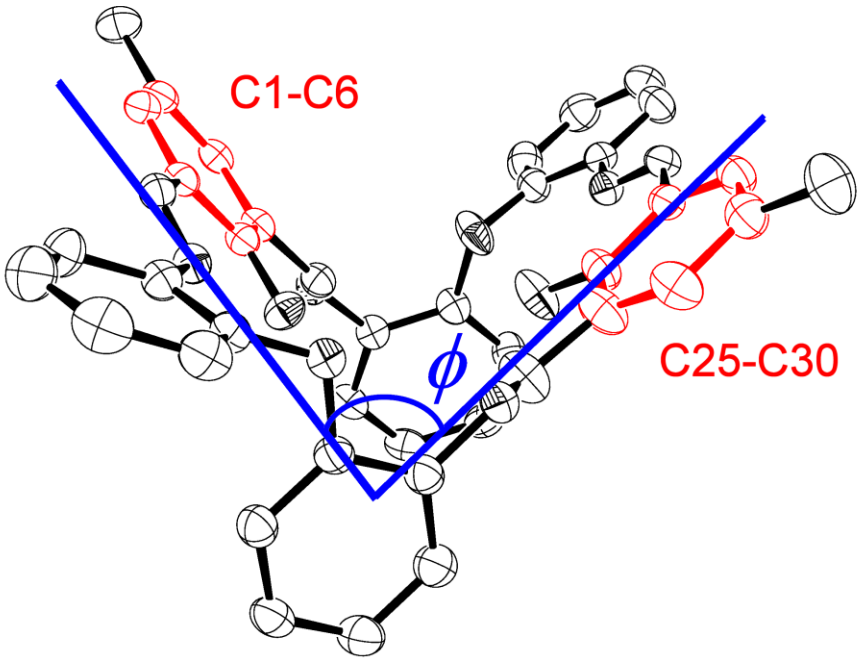

Figure 2. The cleft ϕ, defined by the angle subtended by the mean planes of the phenolate rings.

Intermolecular face-to-face interactions give rise to stacks along the *c* direction (see Figure 3).

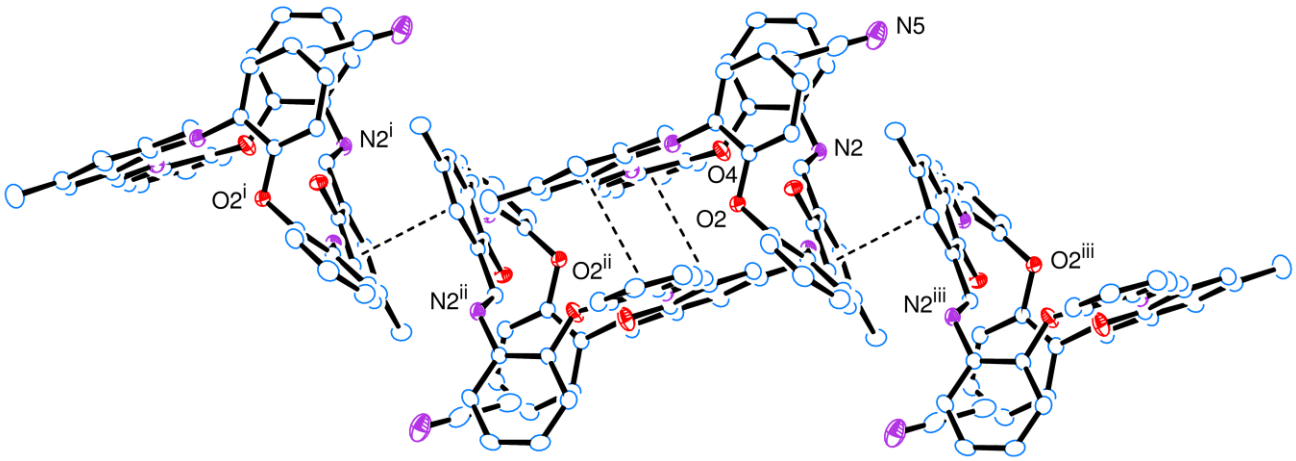

Figure 3. Stacking of $\mathbf{L}^{1}H_2$ molecules parallel to the *c* axis.

In the case of $\mathbf{L^2}H_2$·MeCN, there are two very similar, independent molecules in the crystal, together with two molecules of solvent (MeCN), both of which are disordered in several orientations. In this case, the conformation in each macrocyclic molecule is much more closed with ϕ angles of about 13 and 15 ^{o}, *i.e.* the two sides of the cleft are almost parallel. The whole molecule shows approximate symmetry about a pseudo two-fold axis (see Figures 4 and 5). The pseudo symmetry axes of the two molecules are not parallel. Distinct from $\mathbf{L^1}H_2$·MeCN, the solvent does not reside in a pocket and has no close interaction with the macrocyclic ring. As expected, the bond lengths in $\mathbf{L^2}H_2$·MeCN are similar to those observed in $\mathbf{L^1}H_2$·MeCN, and in each molecule of $\mathbf{L^2}H_2$·MeCN, the hydroxyl hydrogen atoms of the phenol groups were all located from difference maps and refined well to show clear intramolecular hydrogen bonding with neighbouring imine nitrogen atoms [molecule 1: H(1o)–N(1) = 1.57(3) Å and O(1)–H(1o)···N(1) = 150(3) ^{o}, H(3o)–N(3) = 1.79(3) Å and O(3)–H(3o···N(3) = 148(3) ^{o}; molecule 2: H(51o)–N(51) = 1.68(3) Å and O(1)–H(51o)···N(51) = 148(3) ^{o}, H(53o)–N(53) = 1.64(3) Å and O(3)–H(53o)···N(53) = 150(3) ^{o}].

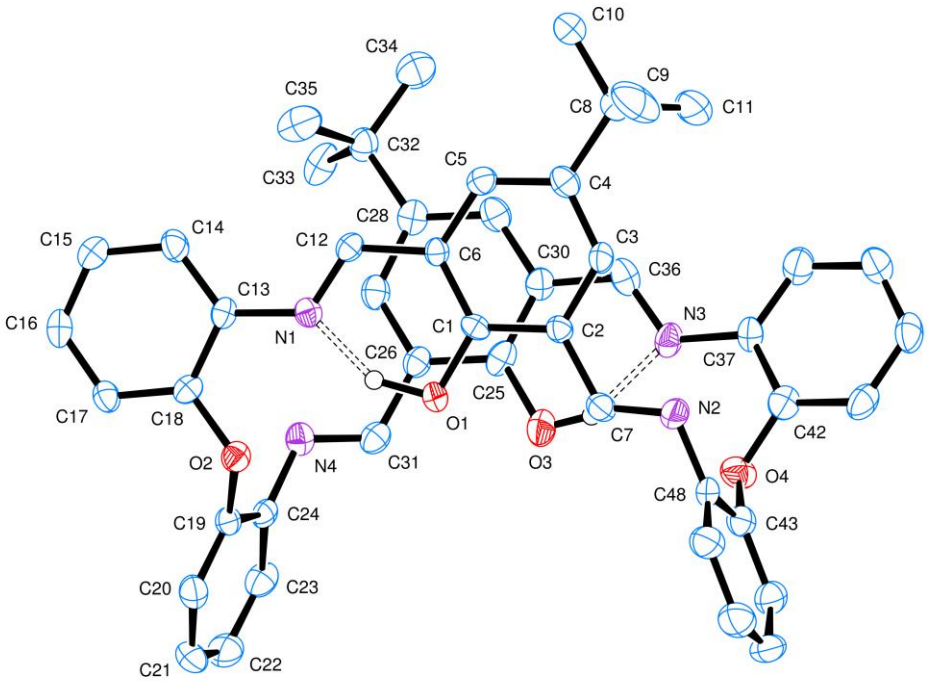

Figure 4. A general view of one molecule of $\mathbf{L}^{2}H_2$·MeCN, indicating the atom numbering scheme. The second molecule is similar. H atoms not involved in H-bonding and the two disordered MeCN molecules are omitted for clarity.

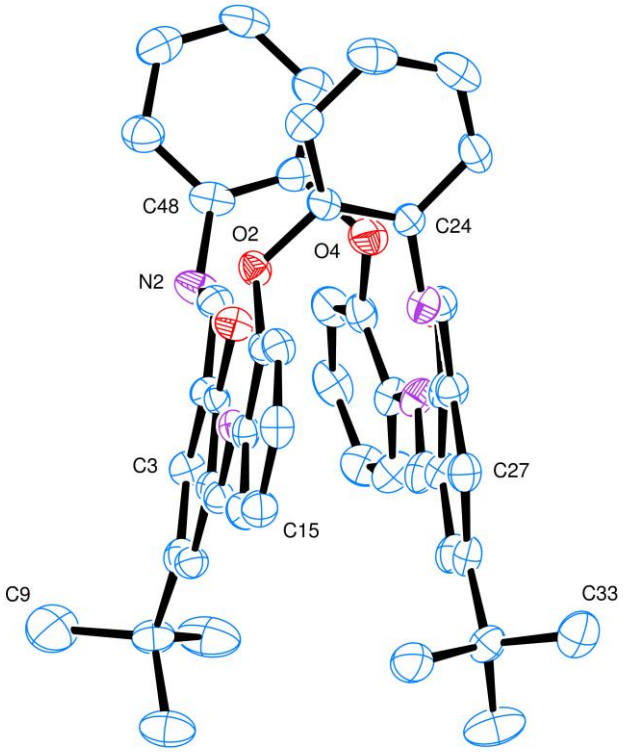

Figure 5. An 'end-on' view of one molecule of $\mathbf{L^2}H_2$·MeCN illustrating the sides of the cleft being almost parallel.

Table 1. Comparison of selected geometrical parameters for solvates of $\mathbf{L^2}H_2$.

	$\mathbf{L^2}H_2$·MeCN	$\mathbf{L^2}H_2$·EtOAc	$\mathbf{L^2}H_2$·2acetone	$\mathbf{L^2}H_2$·2toluene
N(1)-C(12)	1.286(3)	1.288(2)	1.280(2)	1.282(3)
N(1)-C(13)	1.412(3)	1.4188(19)	1.4112(18)	1.415(3)
N(2)-C(7)	1.258(3)	1.2679(19)	1.2616(19)	1.276(3)
N(2)-C(24'/48)	1.411(3)	1.412(2)	1.417(2)	1.422(3)
C(18)-O(2)	1.395(3)	1.3971(19)	1.385(2)	1.392(3)
O(2)-C(19)	1.401(3)	1.4022(19)	1.398(2)	1.391(3)
C(18)-O(2)-C(19)	116.3(2)	115.40(11)	117.10(12)	116.45(19)
C(12)-N(1)-C(13)	123.2(3)	119.70(13)	121.71(15)	120.45(19)
N(2)-C(7)-C(2)	122.5(3)	121.67(14)	123.80(16)	122.6(2)
N(1)-C(12)-C(6)	120.0(3)	122.75(14)	121.78(15)	121.4(2)
C(14)-C(13)-N(1)	126.1(3)	123.87(14)	124.09(15)	124.1(2)
C(18)-C(13)-N(1)	116.0(3)	118.50(14)	117.58(15)	117.1(2)
C(7)-N(2)-C(24'/48)	116.6(3)	119.29(14)	116.98(15)	117.05(19)

$\mathbf{L}^2H_2$ can also be readily crystallized from ethyl acetate from which two different solvates were isolated on separate occasions. The molecular structure of one product is shown in Figure 6, with selected bond lengths and angles given in Table 1. The asymmetric unit contains half a molecule of $\mathbf{L}^2H_2$ and half a disordered solvent molecule. The second half of the macrocycle molecule is generated by a two-fold symmetry axis. Again, the macrocycle possesses quite a tight cleft angle ϕ at about 17 ^{o}. As in the previous solvates, there is intramolecular H-bonding involving the phenolic hydrogen and an imino nitrogen [H(1o) – N(1) = 1.75(2) Å and O(1) – H(1o) $\cdots$ N(1) = 153(2) ^{o}]. The disordered ethyl acetate solvent molecule resides over an inversion centre, and is located in a pocket between four of the macrocycles.

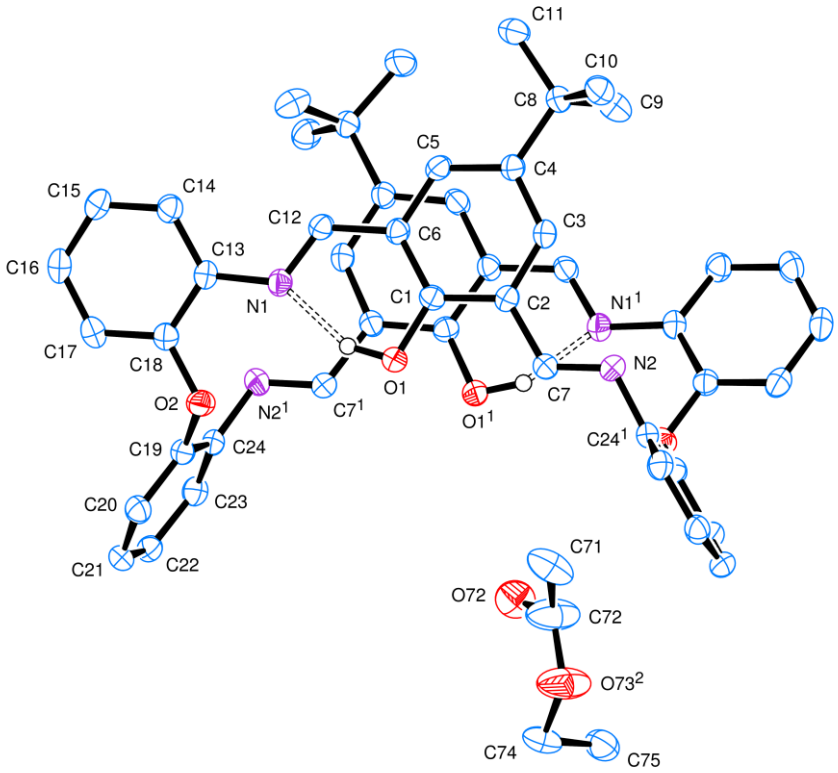

Figure 6. A view of a molecule of $\mathbf{L}^2H_2$·ethyl acetate, indicating the atom numbering scheme. H atoms not involved in H-bonding and the second disorder component of the ethyl acetate molecule are omitted for clarity.

A separate crystallization afforded a different solvate, namely $\mathbf{L^2}H_2\cdot$2(ethyl acetate), the asymmetric unit for which (not shown) contains half a molecule of the macrocycle and one solvent molecule. The main difference from the mono-solvate is that there is a pronounced twist about the central bond, resulting in a C(12)–N(1)–C(13)–C(14) torsional angle of –33.1(8) ^{o} (the same angle in the mono-solvate is –15.8(2) ^{o}). The ϕ angle of the V-shaped cleft in $\mathbf{L^2}H_2\cdot$2(ethyl acetate) is about 7 ^{o} (*i.e.* close to parallel), though it should be noted here that the distance between the rings of each side of the cleft (see Figure S1, ESI) is larger than in the mono-solvate, with a mean of 3.7 Å (*cf* 3.5 Å for the mono-solvate).

In the case of the crystallization from acetone, the asymmetric unit contains half a macrocycle and one molecule of acetone. A similar conformation (Figure 7) to the ethyl acetate solvate is adopted in that the V-shaped cleft has a very tight angle (*ca*. 8 ^{o}). Pairs of acetone molecules, arranged as centrosymmetric dimers, reside in approximately spherically shaped pockets formed between the macrocycle molecules. Again, there is intramolecular H-bonding involving the phenolic hydrogen and an imino nitrogen [H(1o)–N(1) = 1.68(2) Å and O(1)–H(1o)···N(1) = 151(2) ^{o}].

The two different ethyl acetate solvates and the acetone solvate all crystallize in similar sized and shaped unit cells in space group *C*2/*c*; i.e. they are almost isomorphic (see Table 5 for unit cell geometry).

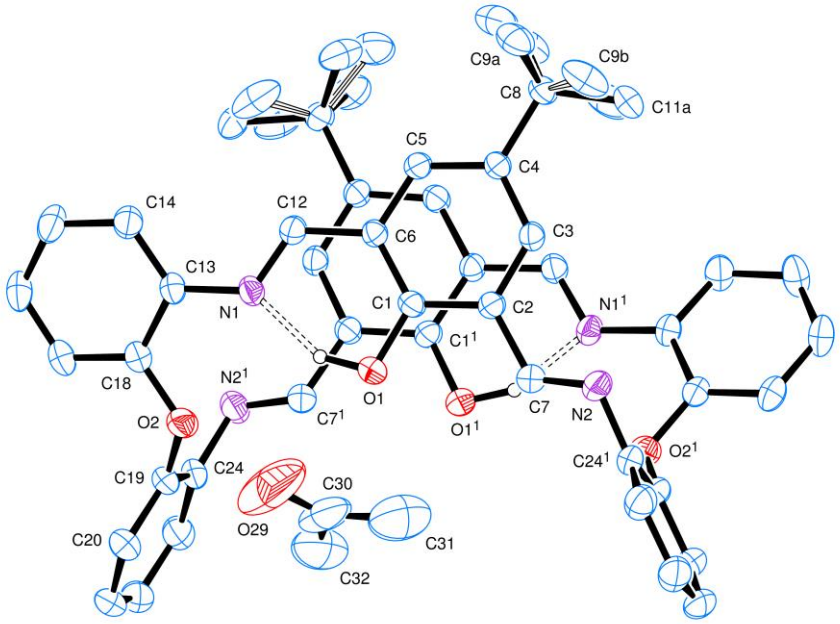

Figure 7. A view of one molecule of $\mathbf{L}^{2}H_2 \cdot 2$(acetone), indicating the atom numbering scheme. H atoms not involved in H-bonding and minor *t*Bu group disorder components have been omitted for clarity.

For the toluene solvate (Figure 8 and Table 1), the asymmetric unit contains a single macrocycle and two unique solvent molecules. In this case, the conformation adopted by the macrocycle is more open such that the 'cleft' has an approximate ϕ angle of 89 ^{o}. This open conformation allows for the formation of π···π and CH···π interactions. The phenyl rings do not directly overlay, rather they are somewhat slipped such that a C–C bond in one ring is positioned directly below the centroid of an adjacent ring (see Figure S2, ESI). The shortest C to centroid distances are 3.38 and 3.42 Å. Intramolecular H-bonding is present involving the phenolic hydrogen and an imino nitrogen [H(1o)–N(1) = 1.74(3) Å and O(1)–H(1o)···N(1) = 150(3) ^{o}, H(3o)–N(3) = 1.66(3) Å and O(1)–H(3o)···N(3) = 151(3) ^{o}].

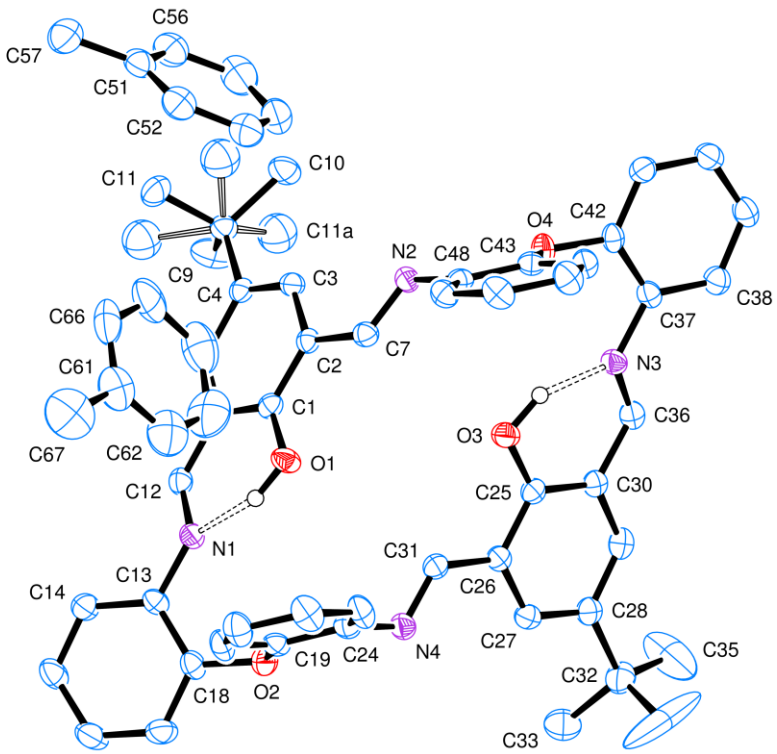

Figure 8. A view of a molecule of $\mathbf{L}^{2}H_2$·2(toluene), indicating the atom numbering scheme. H atoms not involved in H-bonding and minor *t*Bu group disorder components have been omitted for clarity.

In these solvates, the range of C=N bond lengths **(**1.258(3) – 1.288(2) Å, see Table 1 and caption for Figure 1) compares favourably with those reported for the related ethylene bridged phenolic macrocycles [1.2554(17) – 1.299(7) Å], [7b] and those observed in bis(imino)pyridine containing macrocycles [1.246(3) – 1.289(3) Å]. [14]

In these $\mathbf{L}^{2}H_2$ derived systems, the angular variation in the V-shaped cleft can also be gauged by the gradation of tilting of the *t*-butyl-phenol groups, from 6.09(8) ^{o} in $\mathbf{L}^{2}H_2$·MeCOOEt, through $L^{2}H_2$·2(MeCOOEt) at 6.8(2) ^{o}, $\mathbf{L}^{2}H_2$·2acetone at 7.39(7) ^{o}, $\mathbf{L}^{2}H_2$·MeCN at 9.49(14) and 12.56(12) ^{o} in the two molecules (for further analysis see table S1, ESI). By contrast, for the $\mathbf{L}^{1}H_2$ systems, the

structures are more open, for example $\mathbf{L^1}H_2\cdot$MeCN at 89.03(5) °, $\mathbf{L^2}H_2\cdot$2toluene at 89.88(7), and $\mathbf{L^2}$(tosyl)$_2$ at 180.0 °, where the two phenolate rings are opposed and related by a centre of symmetry.

Tosylated macrocycle

The precursor 2,6-dicarboxy-4-R-phenol was prepared *via* tosylation of the parent tris(hydroxyl) compound 2,6-dimethanol-4-R-phenol, and during these syntheses, we isolated one of the tosylated intermediates, which was subsequently reacted with oxydianiline. The resulting tosylated macrocycle $\mathbf{L^2}$(tosyl)$_2$ was crystallized from acetonitrile. The molecular structure is shown in Figure 9 (and an alternative view is given in Figure S3 in the ESI), with selected bond lengths and angles given in the caption. There is half a molecule in the asymmetric unit, and the molecule lies on an inversion centre. In the packing of the molecule, there is off-set π···π stacking: C(1)···C(2') = 3.700 Å, C(2)···O(1') = 3.456 Å, C(6)···C(7') = 3.684 Å.

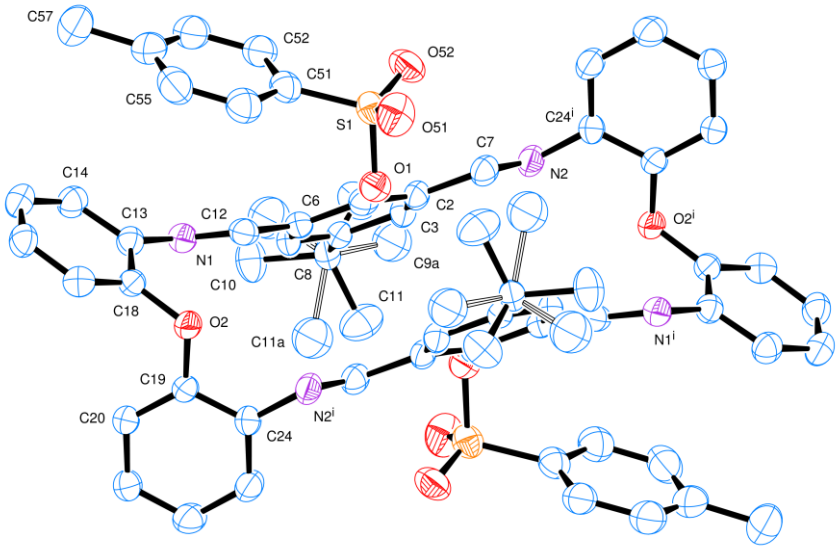

Figure 9. Molecular structure of $\mathbf{L^2}$(tosyl)$_2$. Selected bond lengths (Å) and angles (°): S(1)–O(51) 1.417(2), S(1)–O(52) 1.423(2), S(1)–O(1) 1.620(2), N(2)–C(7) 1.256(4), N(2)–C(24') 1.419(4), N(1)–

C(12) 1.268(4), N(1)–C(13) 1.421(4); C(51)–S(1)–O(1) 105.14(14), N(2)–C(7)–C(2) 121.4(3), N(1)–C(12)–C(6) 120.0(3) °. H atoms and minor tBu group disorder components have been omitted for clarity.

Emission studies

The 'dried' macrocycle was strongly luminescent as a solid with an emission maximum at 585 nm. The Schiff base was also dissolved in a number of solvents, in order of decreasing dipole moment: acetonitrile (3.92), acetone (2.88), ethyl acetate (1.78), dichloromethane (1.60), and toluene (0.37).

The samples were excited at 400 nm, and the emission spectra for $\mathbf{L^1}H_2$, $\mathbf{L^2}H_2$ and $\mathbf{L^3}H_2$ are shown in Figures 10 (a), (b) and (c), respectively. In the case of $\mathbf{L^3}H_2$, the emission spectrum displays the full hypochromic shift of the macrocycle emission in different solvents, from λ_{max} at 508 nm (in acetonitrile) to 585 nm (in CH_2Cl_2); in most cases, components at both 508 and 585 nm are visible. For $\mathbf{L^3}H_2$, in acetonitrile the former (508) is far more pronounced, whilst for $\mathbf{L^1}H_2$, the 508 component is visible in MeCN, acetone and ethyl acetate; in all cases the 508 component is more pronounced in order of increasing dipole moment. The emission is typically broad, with full width at half maximum (FWHM) of 67±2 nm. Typically, the solutions with the largest dipole (acetonitrile) emit towards the blue/green end of the spectrum, whilst the macrocycle in the less polar solvents emits in the red end of the visible spectrum. Given this, we extended our studies to DMSO (dipole moment 3.96), for which the wavelengths exhibited peaks at a) 490 and 588 nm, b) 520 nm and c) 520 and 578 nm, for $\mathbf{L^{1\text{-}3}}H_2$ respectively, results which were consistent with the observed dipole *versus* emission trend.

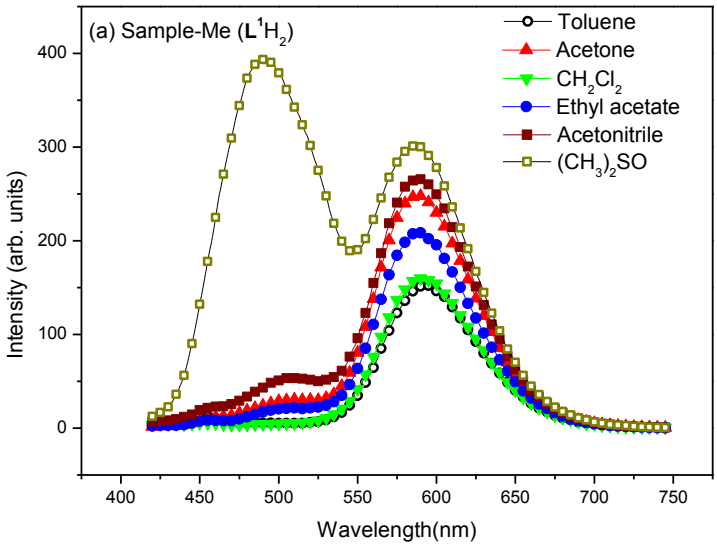
(a) Sample-Me (L^1H_2)
Toluene
Acetone
CH_2Cl_2
Ethyl acetate
Acetonitrile
$(CH_3)_2SO$
Intensity (arb. units)
Wavelength(nm)
0
100
200
300
400
400
450
500
550
600
650
700
750

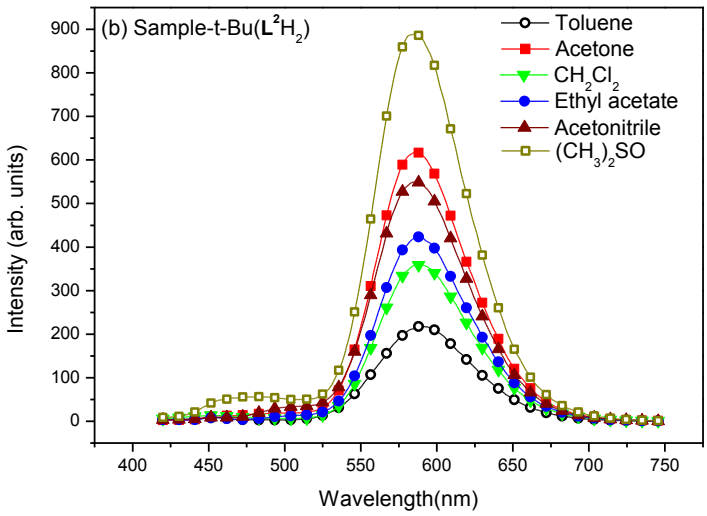
(b) Sample-t-Bu(L^2H_2)
Toluene
Acetone
CH_2Cl_2
Ethyl acetate
Acetonitrile
$(CH_3)_2SO$
Intensity (arb. units)
Wavelength(nm)
0
100
200
300
400
500
600
700
800
900
400
450
500
550
600
650
700
750

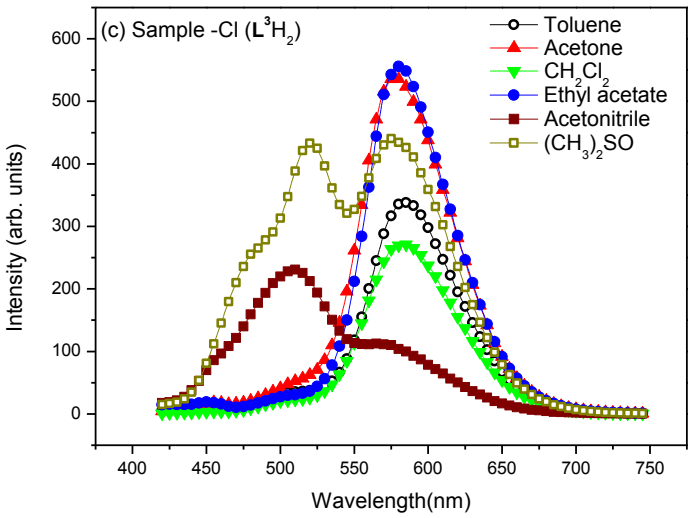

Figure 10. Photoluminescence emission spectra from samples (a) $\mathbf{L^1}H_2$, (b) $\mathbf{L^2}H_2$, and (c) $\mathbf{L^3}H_2$ in various solvents.

For quantum yields (in toluene), see ESI, table S2; the quantum yield of $\mathbf{L^3}H_2$ is the highest, whilst those of $\mathbf{L^1}H_2$ and $\mathbf{L^2}H_2$ are similar.

Preparation, structure and ROP behaviour of organoaluminium complexes

The reaction of the [2 + 2] macrocyclic Schiff bases $\{[2\text{-}(OH)\text{-}5\text{-}(R)C_6H_2\text{-}1,3\text{-}CH][O(2\text{-}C_6H_4N)_2]\}_2$ (R = Me $\mathbf{L^1}H_2$, *t*Bu $\mathbf{L^2}H_2$, Cl $\mathbf{L^3}H_2$) with two equivalents of R'_3Al in refluxing hexane afforded, following work-up, cooling and prolonged standing (1 - 2 days) at ambient temperature, yellow crystals in good yield (*ca*. 55 - 67 %) of the dinuclear complexes $[(AlR'_2)_2L]$ ($\mathbf{L^1}$, R′ = Me (**1**), $\mathbf{L^2}$, R′ = Me (**2**), $\mathbf{L^3}$, R′ = Me (**3**), $\mathbf{L^1}$, R′ = Et (**4**), $\mathbf{L^2}$, R′ = Et (**5**), $\mathbf{L^3}$, R′ = Et (**6**)). Unfortunately, we were unable to grow single crystals of **1** – **6** suitable for X-ray crystallography, and so our attention turned to systems derived from the ethylene-bridged dianiline $[(CH_2CH_2)(2\text{-}C_6H_4NH_2)_2]$ prepared under the same conditions. In

previous work, we have investigated the reaction of two equivalents of R'_3Al with such [2+2] Schiff-base macrocycles, but no structural information was reported. Herein, for R' = Me, we were able to isolate and structurally characterized a secondary product, namely $[(AlMe)(AlMe_2)\mathbf{L}^5]\cdot 2^1/_4MeCN$ (**7**). Small, *orange*, plate-like crystals were grown from a saturated acetonitrile solution on prolonged standing at ambient temperature. The crystals proved to be weakly diffracting, even when using synchrotron radiation, and so data was only integrated to $2\theta = 45^{o}$. The asymmetric unit contains two macrocyclic complexes and 4.5 molecules of solvent of crystallization (MeCN). The molecular structure of one of the macrocyclic structures in shown in Figure 11, with selected bond lengths and angles given in the caption. The interesting features of this complex are i) the different degree of alkylation of the distorted tetrahedral aluminium centres, with Al1 bearing two methyl groups, whereas Al2 has only one, and ii) the '*trans*' positioning of the Al centres. Thus for Al(1), the macrocycle binds in *N*,*O*-bi-dentate fashion, whereas for Al2, the macrocycle coordinates via a tri-dentate *N*,*N*,*O* mode. The conformation of the macrocycle is somewhat twisted to accommodate the tridentate nature of the bonding at Al2.

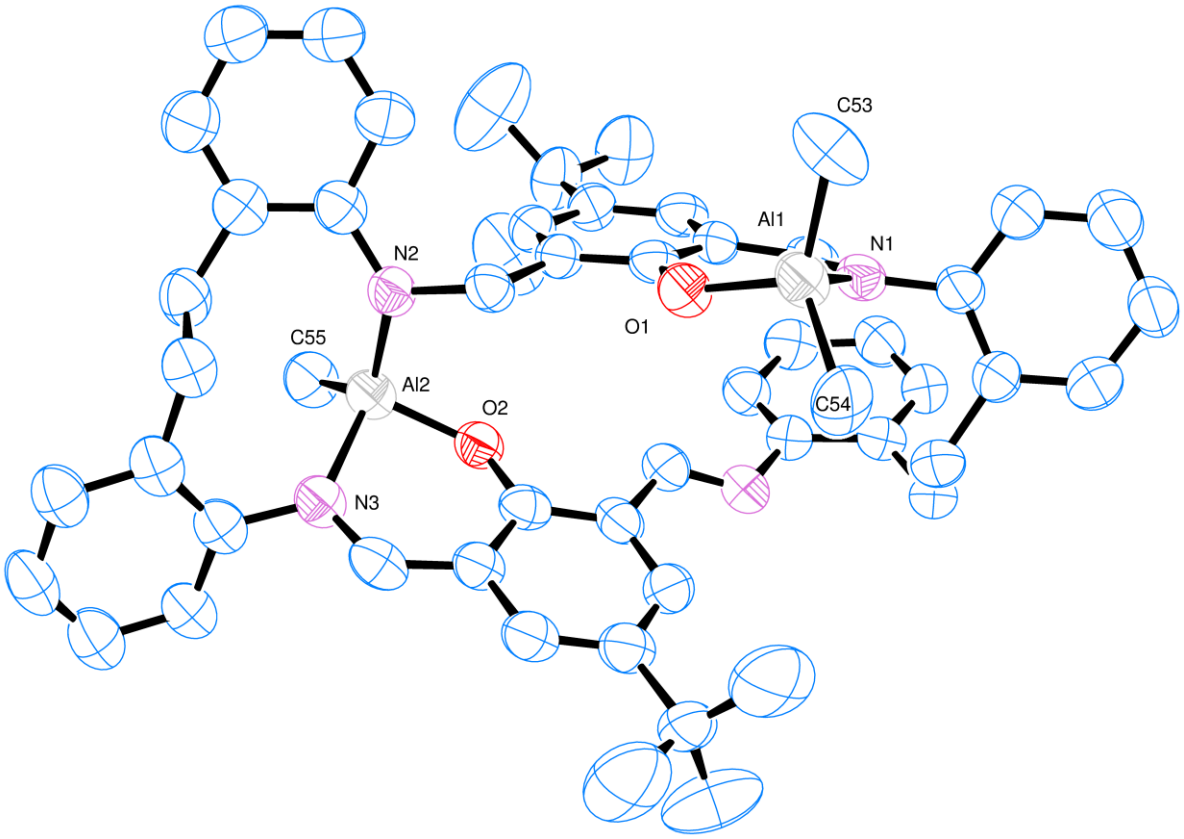

Figure 11. Molecular structure of [(AlMe)(AlMe$_2$)**L**$^{/}$]·2$^1/_4$MeCN (**7**, R = *t*Bu) (**7**), with atoms drawn as 50 % probability ellipsoids. Hydrogen atoms and MeCN of crystallisation have been omitted for clarity. This is one of two similar macrocyclic complexes in the asymmetric unit. Selected bond lengths (Å) and angles (^{o}): Al1 – O1 1.761(4), Al1 – N1 1.963(5), Al1 – C53 1.977(6), Al1 – C54 1.949(5), Al2 – O2 1.768(4), Al2 – N2 1.860(4), Al2 – N3 1.970(4), Al2 – C55 1.963(5); O1 – Al1 – N1 94.49(17), C53 – Al1 – C54 119.3(3), N2 – Al2 – N3 110.9018, O2 – Al2 – C55 109.2(2).

Given the unexpected nature of complex **7**, we re-visited the complex {(Et$_2$Al)[2-(O)-5-(Me)C$_6$H$_2$-1,3-CH][CH$_2$CH$_2$(2-C$_6$H$_4$N)$_2$]}$_2$ (**8**) and determined the centro-symmetric molecular structure of crystals grown from a saturated acetonitrile solution, see Figure 12 and Table 5. Interestingly, again the

structure reveals a '*trans*' deposition of the distorted tetrahedral aluminium centres, though in this case there is the anticipated diorganoaluminium present. Each is bound to the two opposite phenolic oxygen atoms and to a neighbouring imine nitrogen (N1 or $N1^{i}$). The conformation of the macrocycle is relatively planar. The observed '*trans*' deposition of the diethylaluminium centres in **8** could be explained in terms of steric effects, but the situation in **7** is less clear.

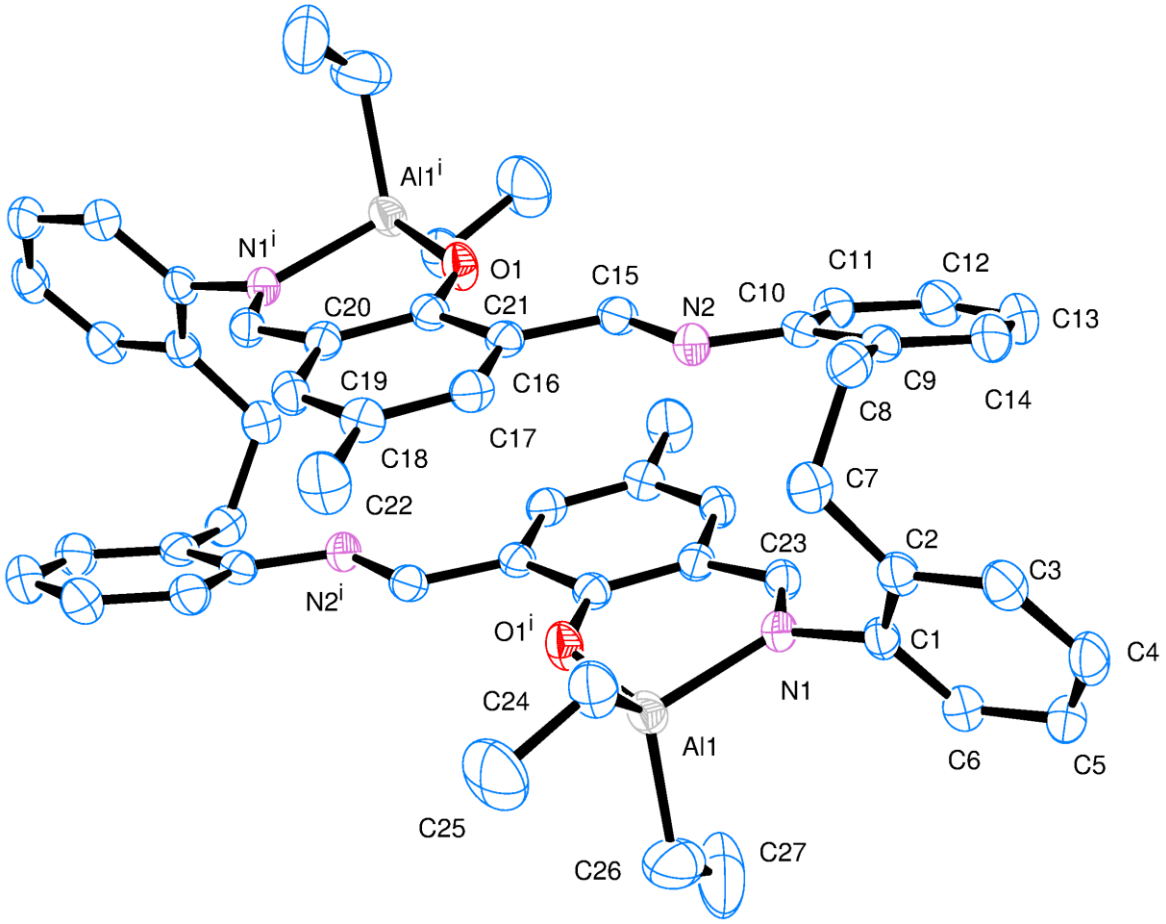

Figure 12. Molecular structure of $[(AlEt_2)_2\mathbf{L}^{4}]$ (**8**), with atoms drawn as 50 % probability ellipsoids. Symmetry operator used to generate the second half of the molecule: *i* = 1-x, -y, 1-z. Hydrogen atoms and MeCN of crystallisation have been omitted for clarity. Selected bond lengths (Å) and angles (°):

Al1 – N1 1.9710(16), Al1 – $O1^{i}$ 1.7826(13), N1 – C23 1.294(2), N12 – C15 1.276(2); N1 – Al1 – $O(1^{i})$ 94.67(6), N1 – Al1 – C26 106.37(10).

Conducting the reaction of $\mathbf{L^3}H_2$ with limited Et_3Al resulted in the isolation of a yellow crystalline material. Crystals grown from a saturated solution of toluene were found to be a bis-chelate structure [Al($\mathbf{L^3}$)($\mathbf{L^3}$H)]·4toluene (**9**·4toluene) (see Figures 13, Tables 2 and 5), in which a distorted octahedral aluminium centre is bound to two of the macrocyclic ligands.

The asymmetric unit contains one complex and four toluene molecules. The central octahedral Al centre is bound by two macrocycles, with one of the macrocycles binding through two atoms [O1 and N1 to form a nearly planar 6-membered chelate ring; the remainder of this macrocycle adopts a taco-like configuration. The remaining coordination sites at aluminium are occupied by two pairs of O/N chelators (both from the other macrocycle), again forming six membered rings that are close to planar. These two chelate rings are linked by a phenyl ring and a single oxo bridge, and are approximately perpendicular at the aluminium. The remainder of this macrocycle adopts a bowl-shaped conformation. There is a single O–H···N hydrogen bond formed by the unbound phenol present. Within the solid-state, the crystal packing facilitates a large number of non-classical C–H···N and C–H···Cl hydrogen bonds. Four unique, crystallographically resolved, toluene molecules lie between the complexes. There is rotational disorder in their positions but no regions of disordered solvent that could be resolved. There is evidence that C–H···π interactions help to locate the toluene.

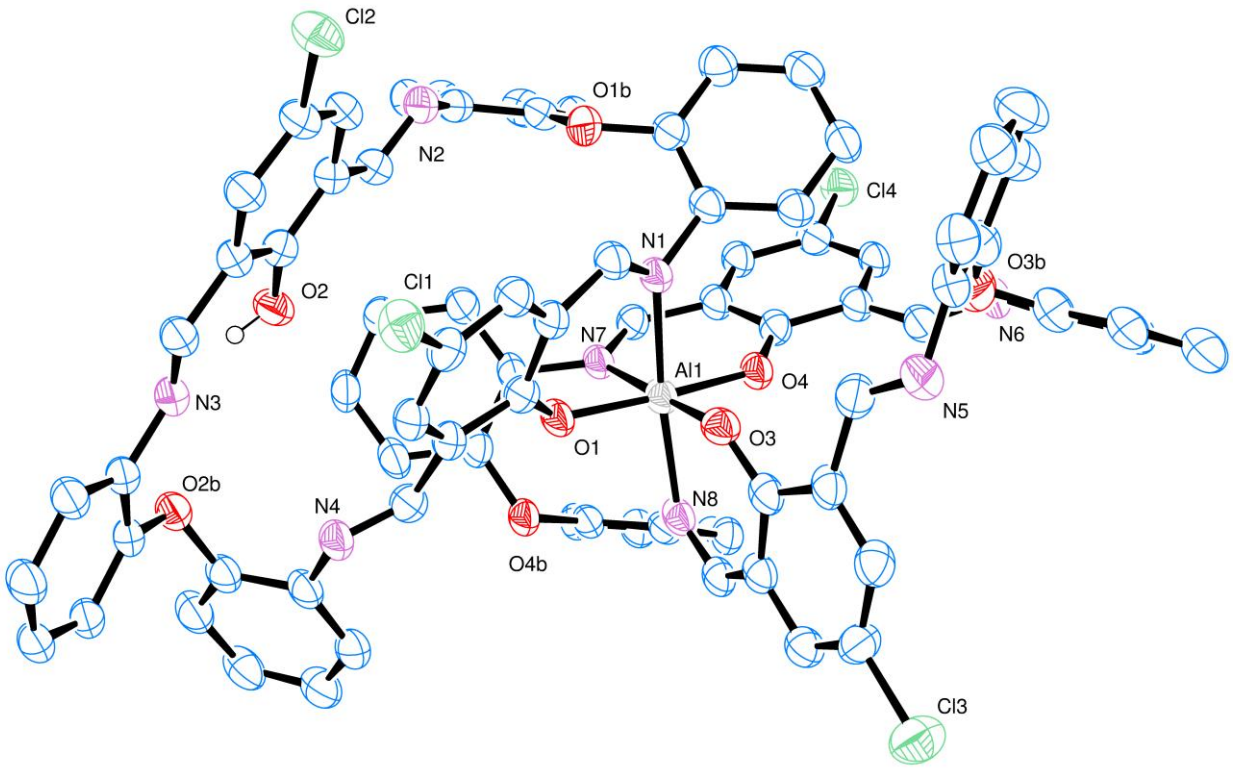

Figure 13. View of the molecular structure of [Al(**L**^{3})(**L**^{3}H)]·4toluene (**9**·4toluene), with atoms drawn as 50 % probability ellipsoids. Hydrogen atoms and toluene molecules of crystallisation have been omitted for clarity.

Table 2. Selected structural data for **9**·4toluene and **10**·5MeCN.

Bond length (Å)/Angle (°)	**9**·4toluene	**10**·5MeCN
Al1–O1	1.8121(17)	1.814(3)
Al1–O3	1.8410(17)	1.819(3)
Al1–O4	1.8338(17)	1.817(3)
Al1–N1	2.100(2)	2.090(3)
Al1–N7	2.079(2)	2.112(4)
Al1–N8	2.114(2)	2.087(3)

O1–Al1–O4	176.18(8)	173.51(16)
O3–Al1–N7	176.96(8)	178.76(14)
N1–Al1–N8	168.76(8)	173.02(15)

Similar treatment of $\mathbf{L}^5H_2$ again afforded a bis-chelate structure, namely [Al($\mathbf{L}^5$)($\mathbf{L}^5$H)]·5MeCN (**10**·5MeCN), for which single crystals suitable for X-ray diffraction were grown from toluene at 0 °C.

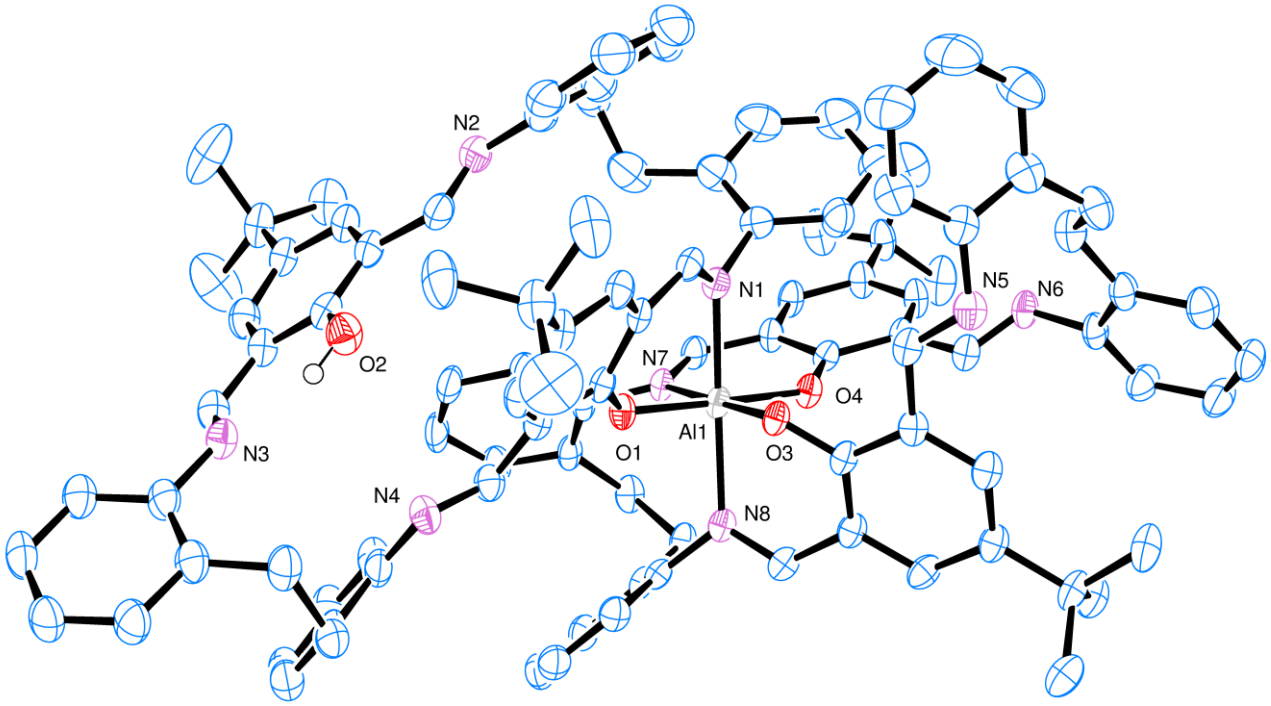

Figure 14. The molecular structure of [Al($\mathbf{L}^5$)($\mathbf{L}^5$H)]·5MeCN (**10**·5MeCN), with atoms drawn as 50 % probability ellipsoids. Hydrogen atoms and MeCN solvent molecules of crystallisation have been omitted for clarity.

The molecular structure of **10**·5MeCN is shown in Figures 14 and S4 and S5 (ESI) which, along with the geometrical parameters (Table 5), reveals the similarity between complexes **9**·4toluene and **10**·5MeCN. The asymmetric unit contains one aluminium complex and 5 molecules of acetonitrile. As for **9**·4toluene, the coordination at the aluminium is such that one macrocycle is bound only in chelate fashion via *N,O*-type ligation, whilst the second macrocycle utilizes four atoms to bind in 2x *N,O*-type fashion. In the bidentate ligand, there is also an intramolecular H-bond involving the phenolic group at O2 and the adjacent imine nitrogen N3. In terms of packing, the aromatic ring at C38 forms a centrosymmetric $\pi\cdots\pi$ interaction at 3.6 Å (see Figure S5, ESI).

Treatment of **L**H_2 with excess R'_3Al (four equivalents) in refluxing hexane afforded, following work-up (extraction into toluene), cooling and prolonged standing (1 – 2 days) at ambient temperature, yellow crystals in moderate yield (*ca* 30 - 35 %) of the tetra-nuclear complexes $[(AlR'_2)_4\mathbf{L}^{1'\text{-}3'}]$ (R = $\mathbf{L}^{2'}$, R' = Me (**11**); $\mathbf{L}^{3'}$, R' = Me (**12**); $\mathbf{L}^{1'}$, R' = Et (**13**); $\mathbf{L}^{3'}$, R' = Et (**14**)), where $\mathbf{L}^{1'\text{-}3'}$ is the macrocycle resulting from double alkyl transfer to imine, namely $\{[2\text{-}(O)\text{-}5\text{-}(R)C_6H_2\text{-}1\text{-}(CH)\text{-}3\text{-}(C(R')H][(O)(2\text{-}(N)\text{-}2'\text{-}C_6H_4N)_2]\}_2$. In the case of the reaction involving $\mathbf{L}^1H_2$ and Me_3Al, single crystals of the complex were grown from a saturated hexane/toluene (50:50) solution at 0 ^oC. The molecular structure is shown in Figure 15, with selected bond lengths and angles given in the caption. This reveals the formation of a tetra-nuclear complex (**11**) akin to that formed form when using the analogous – CH_2CH_2-bridged Schiff-base macrocycle. [15] For a relatively simple compound, the crystal structure displays unwelcome complexity. There are four, symmetry unique, bowl-shaped molecules of **11**·1¾toluene·$1^1/_4$hexane occupying the asymmetric unit. Each of these binds four $AlMe_2$ units; subtle differences in the configuration of the macrocycles render these symmetry independent. Between these macrocycles lie crystallographically resolved and unresolved solvent to give an estimated formula (after Squeeze) [16] of $8\{(Me_2Al)_4[2\text{-}(O)\text{-}5\text{-}(t\text{Bu})C_6H_2\text{-}1\text{-}CH\text{-}3C(Me)H][O(2\text{-}$

$C_6H_4N)_2]\}_2 \cdot 14$toluene·9hexane. To simplify the discussion of the four similar units, the orientation of one macrocycle will be discussed. The macrocycle is twisted such that one *tert*-butyl group is pointing 'up' and one 'down'. At the opposite end of each of the phenyl groups bearing the *tert*-butyl are bound two $AlMe_2$ units. Each aluminium is coordinated by two methyl groups and one neutral imine and a phenoxide in approximately tetrahedral geometry. The phenoxide bridges between the two aluminium centres (atoms O1 and O3 in Figure 15). One pair of aluminium atoms reside on one side of the molecule and the others lie on the opposite side. There is evidence for C–H···π interactions between adjacent macrocycles but the packing is unremarkable. Between the macrocycles lie ordered and disordered solvent; some hexane and toluene are crystallographically resolved. There are also portions of the structure in which the solvent molecules cannot be located reliably and these regions were modelled using the Squeeze routine. [16]

The formation of **11** involves an intramolecular regioselective methyl transfer to two imine moieties of the macrocycle; such methyl transfers are now well established in imine chemistry. [17] The methyl transfer occurs at imine groups originating from the same dianiline. In the ^{1}H NMR spectra of **11**, the Me – Al resonances occur as eight singlets between –0.52 and –1.39 ppm (and four singlets between –0.49 and –1.01 for **12**). In the case of the related ethyl derivatives **13** and **14**, two of the Al-Et groups appear to be subject to ring currents which result in unusual low field chemical shifts in the ^{1}H NMR spectra for the CH_2 protons (see experimental section).

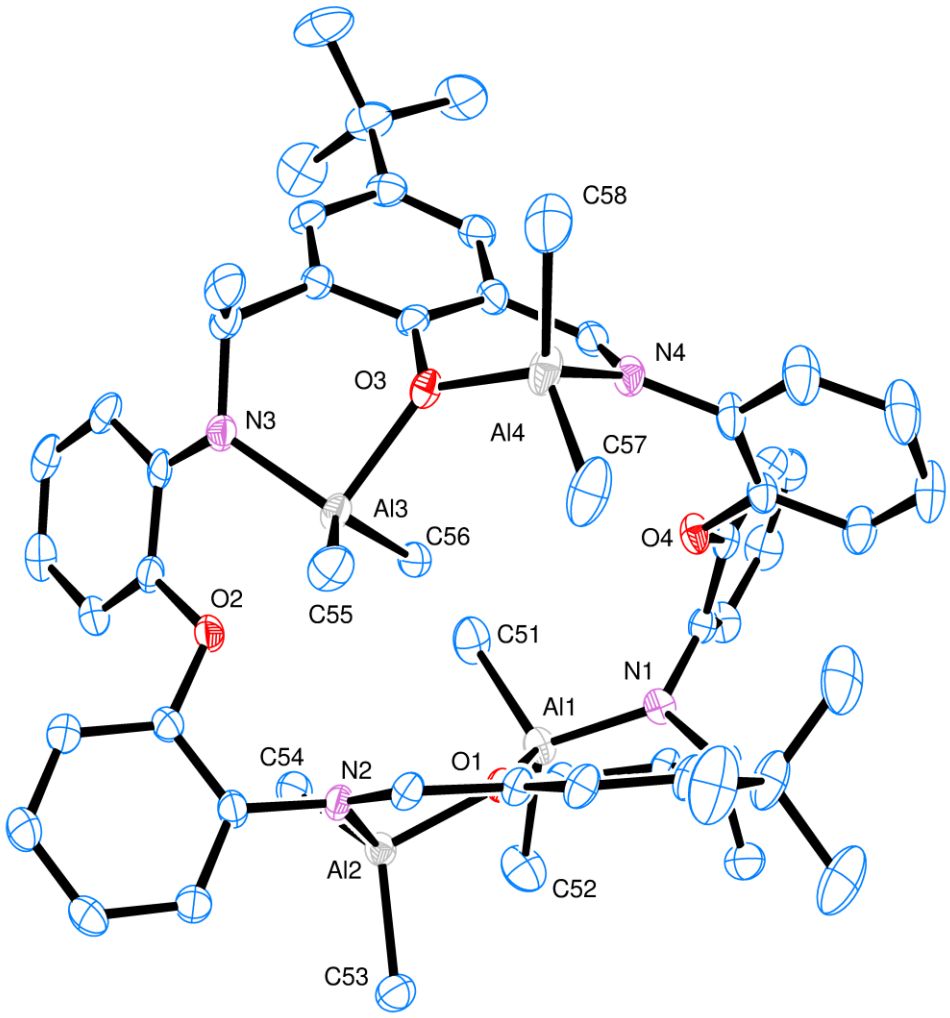

Figure 15. Molecular structure of $[(AlMe_2)_4L^{1/}]\cdot 1¾$toluene$\cdot 1^1/_4$hexane (**11**$\cdot 1¾$toluene$\cdot 1^1/_4$hexane), showing the atom numbering scheme. Hydrogen atoms and solvent molecules of crystallisation have been omitted for clarity. This is one of four unique complex molecules in the asymmetric unit. Selected bond lengths (Å) and angles (°): Al1 – N1 1.820(3), Al1 – O1 1.950(2), Al2 – O1 1.857(2), Al2 – N2 1.952(2), Al3 – O2 2.430(2), Al3 – O3 1.997(2), N1 – C1 1.469(4), N2 – C13 1.286(4), N2 – C15 1.276(2), N2 – C14 1.442(4), N3 – C25 1.381(4), N3 – C26 1.473(4), N4 – C38 1.288(4), N4 – C39, Al1···Al2 3.1695(12), Al1···Al3 5.8984(13), Al1···Al4 7.3100(13), Al2···Al3 5.0994(13), Al2···Al4

7.5339(13), Al3···Al4 3.4600(13); Al1 – O1 – Al2 112.73(10), Al3 – O3 – Al4 129.79(12), N1 – Al1 – O1 95.53(10), O1 – Al2 – N2 94.72(10).

Ring opening polymerisation (ROP) of ε-caprolactone and rac-lactide

The dinuclear alkylaluminium complexes **1** – **6** and the tetranuclear alkylaluminium complexes **11** – **14** have been screened for their ability to ring open polymerise ε-caprolactone (see Tables 3 and S3) and *rac*-lactide (Tables 4 and S4). Results are compared against the known $–CH_2CH_2–$ bridged complexes **15** and **16**.

ROP of ε-caprolactone: Runs were conducted both in the presence and absence of benzyl alcohol (BnOH). Complex **5** was used to determine the optimized conditions (Table 3). On increasing the temperature from 20 to 110 ^{o}C and using 250:1:1 (ε-CL:cat:BnOH) over 30 min (runs 1 - 4, Table 3), the % conversion dramatically increased, reaching around 98% conversion at 80 ^{o}C and then increasing only slightly on further elevating the temperature to 110 ^{o}C. Under the same conditions, the molecular weight (M_n) peaked at 80 ^{o}C. All the polycaprolactone polymers (PCLs) obtained possessed a narrow distribution/polydispersity index (PDI) with unimodal characteristics [M_w/M_n = 1.12 – 1.58]. The drop off in molecular weight at 110 ^{o}C results in a plot of %conversion versus M_n which is only approximately linear. We have also investigated the effect of the ε-CL/Al molar ratio on the catalytic behaviour (entries 3, 8 and 9, Table 3) in the presence of one equivalent of BnOH. When the molar ratio CL:Al was increased from 100 to 500 over 30 min., the molecular weight increased from 2.16 to 4.62×10^4, whilst the conversion rate exhibited the opposite trend peaking at 99.1 % for 100:1:1; the molecular weight distribution increased on increasing the molar ratio CL:Al (from 1.13 to 4.01). On increasing the time from 10 min to 60 min., and using 250:1:1 (CL:Al:BnOH) at 80 ^{o}C (runs 3, 5 – 7, Table 3), the conversion gradually increased with time, whilst the molecular weight (M_n) and

polydispersity (PDI) remained relatively constant, except in the case of run 9 where it was, surprisingly, somewhat broader (4.01). Increasing the amount of BnOH (run 12 *versus* 3, Table 3) was detrimental to the molecular weight (M_n), whilst only slightly narrowing the polydispersity, and lowering the % conversion slightly. Conducting the ROP in the absence of BnOH (run 11 *versus* 3, Table 3) led to a reduction in the % conversion, but afforded a significant increase in the polymer molecular weight (M_n); there was little change in the PDI.

Table 3. ROP of ε-CL using complex **5**

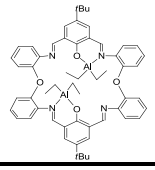

Run	Cat.	CL: Al :BnOH	T/℃	t/min	Conv.%[a]	$Mn\times10^{4}$[b]	$Mn_{Calcd}\times10^{4}$[c]	PDI
1	**5**	250:1:1	20	60	15.8	0.59	0.45	1.08
2	**5**	250:1:1	50	30	64.4	1.57	1.82	1.15
3	**5**	250:1:1	80	30	98.0	3.36	2.82	1.56
4	**5**	250:1:1	110	30	98.5	2.67	2.71	1.58
5	**5**	250:1:1	80	10	59.0	2.98	1.68	1.29
6	**5**	250:1:1	80	20	92.5	3.24	2.63	1.34
7	**5**	250:1:1	80	60	99.2	2.88	2.69	1.40
8	**5**	100:1:1	80	30	99.1	2.16	1.12	1.13
9	**5**	500:1:1	80	30	86.7	4.62	4.94	4.01
11	**5**	250:1:0	80	30	80.1	6.59	2.28	1.60
12	**5**	250:1:3	80	30	93.1	2.02	2.65	1.26

[a] By ^{1}H NMR spectroscopic analysis. [b] Obtained from GPC analysis times 0.56. [c] (F.W.[M]/[BnOH])(conversion)

Complexes **1 - 14** (not **8 - 10**) were then screened using the ratio 250:1:1 (ε-CL:cat:BnOH) over 30 min at 80 ^{o}C, and for comparison, the known complexes **15** and **16** were screened under the conditions employed herein. For the di-nuclear complexes **1 - 6** (runs 1 - 6, Table S3), in terms of the %

conversion, these complexes behave similarly, which does not allow for the observation of any significant structure/activity relationships. Given this, we provide only a brief discussion here and the tabulated data can be found in the ESI (Table S3). For **1** – **6**, the highest conversion was observed for **5** (R = *t*Bu, R$^{/}$ = Et: 98.0 %) and the lowest for **1** (R = R$^{/}$ = Me: 93.2 %). For pairs of complexes where R is constant, the ethyl derivatives were more active than the methyl derivatives and the molecular weights (M_n) were higher; such trends have been noted previously; [18] the opposite trends in activity have also been noted. [19] The spread of molecular weights (M_n) [5.14 - 10.12 × 10^4] also followed no obvious trend, whilst in all cases, the PDI remained relatively constant [1.22 – 1.49]. However, in all cases, the performance of the oxy bridged systems was superior to that of the di-nuclear –CH_2CH_2– bridged complexes **7** and **15**, for which the %conversion was only 25.6% and 38.5%, respectively under the conditions employed herein.

In the case of the tetra-nuclear complexes **11** – **14** (runs 8 – 11, Table S3), the complexes bearing methyl at the *para* position of the phenolic group afforded high conversions of about 99 %, whilst the systems (**12** and **14**), employing a *para* Cl, gave lower conversions of 80.9 and 94.3 %, respectively. This may be attributed to observed solubility issues rather than electronic effects. The polymer molecular weight (M_n) associated with **12** and **14** was also somewhat lower than that observed for the other tetra-nuclear systems. Again, the performance of the related –CH_2CH_2– bridged complex, namely **16** was inferior under the conditions employed herein affording a %conversion of 29.1% and a much lower molecular weight (M_n). This enhanced activity is tentatively ascribed to the ability of the oxygen bridge to stabilize the catalytically active species, akin to the situation observed in dimethyleneoxa-bridged calixarenes systems during ethylene polymerization. [20] As for the di-nuclear systems, the tetra-nuclear ethylaluminium derivatives (**13** and **14**) were more active than the methylaluminium counterparts (**11** and **12**).

In general, the resulting PCL polymer molecular weights were in reasonable agreement with the calculated values, which indicates that there are, in most cases, little in the way of *trans*-esterification reactions occurring. However, in the MALDI-ToF mass spectra, as well as the population of peaks separated by 114.14 mass units (see Figures S6 and S7), there was evidence of a second, albeit minor, population which is more pronounced at 25 ^{o}C. A plot of average molecular weight (M_n) *versus* conversion (Figure S8) exhibited a near linear relationship. In the ^{1}H NMR spectra of the PCL (Figures S9 and S10), signals at around 7.34 and 5.15 ppm ($C_6H_5CH_2$–) and 3.62 (CH_2CH_2OH), with an integral ratio 5:2:2, indicated that the polymer chains are capped by a benzyl group and a hydroxy end group.

ROP of rac-lactide: Complex **5** was again used to verify the optimum condition for the ROP of *rac*-lactide (see Table 4). At 50 ^{o}C, there was no activity (run 6, Table 4), whilst the activity increased on raising the temperature from 80 to 110 ^{o}C. Best conversions at 110 ^{o}C were achieved with the ratio 100:1:1 for *rac*-Lac:Al.BnOH, whilst prolonging the screening time from 6 to 24 h only afforded a slight increase in the % conversion. In all cases, the system was relatively well controlled with polydispersities in the range 1.03 – 1.41.

Table 4. ROP of *rac*-lactide using complex **5**

Run	Lac:M:BnOH	T/℃	t/h	Conv./%[a]	*Mn*×10^{4}[b]	*Mn* Cal×10^{4}[c]	PDI
1	100:1:1	110	1	57.8	0.42	0.83	1.02
2	100:1:1	110	3	91.3	0.63	1.31	1.03
3	100:1:1	110	6	95.0	1.56	1.39	1.21
4	100:1:1	110	12	97.7	1.60	1.40	1.19
5	100:1:1	110	24	98.6	1.45	1.40	1.14
6	100:1:1	50	12	/	/	/	/
7	100:1:1	80	12	66.7	0.74	0.96	1.07
8	50:1:1	110	12	94.3	0.80	0.67	1.41

9	200:1:1	110	12	96.6	2.29	2.78	1.14

[a] By ^{1}H NMR spectroscopic analysis. [b] M_n values were determined by GPC in THF *vs* PS standards and were corrected with a Mark-Houwink factor of 0.58. [c] Polydispersity index (M_w/M_n) were determined by GPC.

Complexes **1** - **14** (not **8** - **10**) were then screened using the ratio 250:1:1 (ε-CL:cat:BnOH) over 30 min at 80 ^oC (Table S4). The ROP appeared to be well controlled in terms of PDI with values in the range 1.07 – 1.38. There was no obvious advantage in the use of di- *versus* tetra-nuclear systems under the conditions employed. For the di-nuclear systems, the ethylaluminium derivatives were slightly more active than their methylaluminium counterparts and the polymers possessed slightly higher molecular weight (M_n), however this trend was not evident for the tetra-nuclear systems. ^{1}H NMR spectroscopic investigations were conducted in order to verify the polymer molecular weights and to identify the end groups present. The results were similar (eg see Figure S11) to the results obtained for the PCL runs, *i.e.* insertion of a benzyloxy group during polymerization. Again, there was reasonable agreement between observed and calculated molecular weights (M_n), whilst MALDI-ToF spectra (e.g. Figure S12) revealed a number of minor populations. To assign the stereochemistry of the PLA polymers, we employed 2D *J*-resolved ^{1}H NMR (e.g. see Figures S13 and S14) and assigned the peaks by reference to the literature. [21] These systems gave moderately isotactic PLA with *P*r values in the range 0.64 – 0.67.

In conclusion, [2+2] Schiff base macrocycles of the type $\{[2\text{-}(OH)\text{-}5\text{-}(R)C_6H_2\text{-}1,3\text{-}(CH)_2][O(2\text{-}C_6H_4N)_2]\}_2$ (R = Me $\mathbf{L^1}H_2$, *t*Bu $\mathbf{L^2}H_2$, Cl $\mathbf{L^3}H_2$) are readily accessible by reacting 2,6-dicarboxy-4-R-phenol with the diamine 2,2′-oxydianiline, $(2\text{-}NH_2C_6H_4)_2O$. The molecular structures of a number of solvates have been determined and their emission properties have been investigated. The molecular structures of the various solvates reveal a tendency to form a taco-shaped conformation, the cleft angle

ϕ associated with the latter varies greatly with that of $\mathbf{L^1}H_2$·MeCN and $\mathbf{L^2}H_2$·2toluene being very open at 103 and 112. ^{o}, respectively, whilst the other solvates (MeCN, acetone and ethyl acetate) of $\mathbf{L^2}H_2$ were more closed with cleft angles ϕ in the range 8 – 17 ^{o}. The solvent is only encapsulated by the macrocycle in $\mathbf{L}^1H_2$·MeCN. Ethyl acetate and acetone reside in similar locations *exo* to the macrocycle in a series of three pseudo-isomorphic structures. Features of the emission can be aligned with the dipole of the solvent system employed. In particular, $\mathbf{L^3}H_2$ exhibited a hypochromic shift of the macrocycle emission in different solvents, from λ_{max} at 508 nm (in acetonitrile) to 585 nm (in dichloromethane). Furthermore, we have found that the interaction of alkylaluminium reagents can be more complicated than originally thought (from studies of the $–CH_2CH_2$- bridged systems) and a number of unexpected products can be formed. In particular, we have found that for the di-nuclear species, '*trans*' as well as the previous '*cis*' structures can readily be isolated, as can complexes in which one of the methylaluminium centres is bound in tridentate fashion by the macrocycle. Moreover, species in which there are no alkyl groups at aluminium, but where two macrocycles bind such that the Al centre is near octahedral, are readily formed in the presence of limited organoaluminium reagent. Tetra-nuclear complexes can be accessed which have undergone alkyl transfer (×2) to one side of the macrocycle by employing excess organoaluminium reagent. These organoaluminium species are capable of the ROP of ε-caprolactone and *rac*-lactide and can out-perform the related systems bearing $–CH_2CH_2–$ bridged Schiff-base macrocycles under similar conditions. However, there appears to be little benefit in the use of di- *versus* tetra-nuclear species under the ROP conditions employed herein.

Experimental

General: Methanol was dried over magnesium. DME was refluxed over sodium and benzophenone. Toluene was refluxed over sodium. Acetonitrile was refluxed over calcium hydride. IR spectra (nujol

mulls, KBr windows) were recorded on a Nicolet Avatar 360 FT IR spectrometer; ^{1}H NMR and ^{13}C NMR spectra were recorded at room temperature on a Varian VXR 400 S spectrometer at 400 MHz or a Gemini 300 NMR spectrometer or a Bruker Advance DPX-300 spectrometer. The ^{1}H NMR spectra were calibrated against the residual protio impurity of the deuterated solvent. Elemental analyses were performed by the elemental analysis service at the London Metropolitan University, the Chemistry Department at the University of Hull or at Sichuan University, Chengdu. The precursors 2,6-$(CHO)_2$-4-R-C_6H_2OH and $(2\text{-}NH_2C_6H_4)_2O$ and 2,2$^{/}$-ethylenedianiline and the complexes **15** and **16** were prepared by the literature methods. [15, 22, 23] The Schiff-base ligands were prepared as outlined below, and the respective solvates were crystallized by taking about 100 mg of the macrocycle and dissolving in the appropriate solvent. In the case of acetonitrile and toluene, the solvates crystallized out at ambient temperature, whereas for acetone and ethyl acetate, cooling to –20 ^{o}C was required. For the organoaluminium complexes, all manipulations were carried out under an atmosphere of dry nitrogen using conventional Schlenk and cannula techniques or in a conventional nitrogen-filled glove box. All solvents were distilled and degassed prior to use.

Synthesis of $\mathbf{L^1}H_2$

2,6-Dicarboxy-4-Me-phenol (0.82 g, 5.0 mmol) and $(2\text{-}NH_2C_6H_4)_2O$ (1.00 g, 5.0 mmol) were refluxed in dry methanol (50 ml) for 12 h in the presence of a few drops of acetic acid. On cooling, the solvent was removed *in-vacuo*, and the residue was extracted into toluene (30 ml). An orange crystalline sample of $\mathbf{L^1}H_2$ was formed on prolonged standing (2 - 3 days) at ambient temperature, yield 1.20 g, 74 %. Single crystals suitable for X-ray crystallography can be grown from a saturated acetonitrile or toluene solution on prolonged standing (slow evaporation) at room temperature. Anal.calcd for $C_{42}H_{32}N_4O_4\cdot C_7H_8$: C, 78.59; H, 5.38; N, 7.48; Found C, 78.77; H, 5.28; N, 7.15 %. IR (cm^{-1}): 3068

(w), 3028(w), 2864(w), 1626(s), 1579(s), 1480(s), 1453(s), 1359(m), 1314(w), 1240(s), 1215 (m), 1195 (m), 1155 (w), 1032 (m), 1008 (m), 854 (m), 837 (m), 786 (m), 745 (s), 700 (w), 65 3(w), 603 (w), 538 (w), 511 (w), 454 (m); MS (EI^+) *m/z*: 657 $[M]^+$. ^{1}H NMR (400 MHz, DMSO-d_6) δ: 14.11 (s, 2H, O*H*), 8.87 (s, 4H, -C*H*=N), 7.54 (s, 4H, Ar-*H*), 7.12 - 7.24 (m, 16H, Ar-*H*), 2.27 (s, 3H, -CH_3), 2.24 (s, 3H, -CH_3). ^{13}C NMR (100 MHz, DMSO-d_6) δ: 20.4, 116.0, 116.6, 117.7, 120.1, 124.2, 127.7, 140.1, 143.6, 149.7, 160.4,

Synthesis of $\mathbf{L^2}H_2$

As for $\mathbf{L^1}H_2$, but using 2,6-bicarboxy-4-*tert*-butyl-phenol (1.03 g, 5.0 mmol) and (2-$NH_2C_6H_4)_2O$ (1.00 g, 5.0 mmol), yield 1.1 g, 60 %. Anal Calcd for $C_{48}H_{44}N_4O_4$ (sample dried *in vacuo* for 12 h): C, 77.81; H, 5.99; N, 7.56; Found: C,77.35; H, 6.43; N, 7.96 %. IR (cm^{-1}): 3063 (w), 2954 (m), 2932 (m), 2864 (w), 1630 (s), 1578 (m), 1484 (m), 1452 (w), 1357 (m), 1316 (w), 1238 (s), 1192 (m), 1158 (m), 1034 (m), 1006 (s), 981 (w), 857 (w), 789 (w), 748 (s), 652 (w), 600 (w), 548 (w), 452 (w). MS (EI^+) *m/z* : 741$[M]^+$. ^{1}H NMR (400 MHz, DMSO-d_6): δ 14.86 (s, 2H, -O*H*), 8.81 (s, 4H, -C*H*=N), 7.25 (s, 4H, Ar-*H*), 7.06 - 7.25 (m, 16H, Ar-*H*), (s, 18H, C(C$H_3)_3$). ^{13}C NMR (100 MHz, DMSO-d_6) δ: 31.7, 34.3, 116.0, 116.8, 118.2, 120.6, 124.2, 125.1, 140. 1, 140.3, 143.6, 160.9.

Synthesis of $\mathbf{L^3}H_2$

As for $\mathbf{L^1}H_2$, but using 2,6-bicarboxy-4-chloro-phenol (0.92 g, 5.0 mmol) and (2-$NH_2C_6H_4)_2O$ (1.00 g, 5.0 mmol), yield 1.4 g, 80 %. $C_{40}H_{26}N_4O_4Cl_2$ (sample dried *in vacuo* for 12 h): C, 68.87; H, 3.76; N, 8.03. Found: C, 69.26; H, 4.16; N, 8.09 %. IR (cm^{-1}): 3063 (w), 2924 (w), 2854 (w), 1627 (s), 1598 (w), 1574 (s), 1540 (m), 1483 (s), 1452 (s), 1369 (w), 1352 (m), 1303 (m), 1238 (s), 1209 (m), 1185 (m), 1155 (w), 1108 (m), 1012 (s), 965 (w), 937 (w), 915 (w), 890 (m), 866 (m), 798 (w), 749 (s), 692

(w), 647 (w), 597 (w), 564 (w), 517 (w), 457 (w), 417 (w). MS(EI^+) *m/z*: 698$[M]^+$. ^{1}H NMR (400 MHz, DMSO-d_6): δ 14.89 (s, 2H, -O*H*), 8.84 (s, 4H, -C*H*=N), 7.58 (s, 4H, Ar-*H*), 7.22-7.34 (m, 12H, Ar-*H*), 7.07 (d, *J* = 11.2 Hz, 4H, Ar-*H*). This compound proved to be too insoluble to obtain meaningful ^{13}C NMR spectra, even upon heating in DMSO-d_6.

Synthesis of $\mathbf{L^2}(tosyl)_2$

The oxydianiline (1.00 g, 4.99 mmol) was combined with 2,6-bicarboxy-4-*tert*-butyl-phenoxytosylate (1.80 g, 4.99 mmol) in ethanol (30 ml) and the system was refluxed for 12 h. The volatiles were removed *in-vacuo*, and the residue was extracted in acetonitrile (30 ml). Prolonged standing at ambient temperature afforded orange crystals of $\mathbf{L^2}(tosyl)_2$ (1.86 g, 71 %). $C_{62}H_{56}N_4O_8S_2$ (sample dried *in vacuo* for 12 h): C, 70.97; H, 5.38; N, 5.34. Found: C, 70.56; H, 5.16; N, 5.09 %. IR (cm^{-1}): 3624 (w), 1927 (w), 1770 (w), 1721 (s), 1620 (s), 1340 (s), 1302 (s), 1261 (s), 1154 (s), 1093 (s), 981 (m), 926 (m), 907 (m), 888 (s), 855 (s), 801 (s), 721 (s), 623 (s), 542 (s), 510 (w), 486 (m). MS (ESI) *m/z*: 895 [MH^+ - tosyl].

Synthesis of $\{(Me_2Al)[2\text{-}(O)\text{-}5\text{-}(Me)C_6H_2\text{-}1,3\text{-}(CH)_2][O(2\text{-}C_6H_4)_2N)_2]\}_2$ (**1**)

To the ligand $[2,2^{/}\text{-}O(C_6H_4N)_2\text{-}2,6\text{-}(4\text{-}MeC_6H_3OH)]_2$ (0.50 g, 0.76 mmol) in hexane was added two equivalents of $AlMe_3$ (0.95 ml, 1.52 mmol), and the system was refluxed for 12 h. The resulting solid was isolated and washed with cold hexane (30 ml) and dried *in vacuo*, to afford **1** as a yellow solid (0.33 g, 56.6 %). Elemental analysis calculated for $C_{46}H_{42}N_4O_4Al_2$: C 71.87, H 5.51, N 7.29 %; found: C 71.62, H 5.47, N 7.11 %. IR (KBr): cm^{-1} 3421 (s), 3063 (w), 3014 (w), 2925 (m), 1625 (s), 1592 (s), 1555 (s), 1484 (s), 1451 (s), 1383 (m), 1371 (m), 1336 (w), 1295 (w), 1238 (s), 1216 (s), 1189 (m), 1110 (m), 1039 (m), 990 (m), 932 (w), 863 (m), 833 (m), 789 (m), 750 (s), 711 (m), 686 (m), 606 (w),

546 (w), 457 (w). MS (E.I.) 723.16 $[M - 3CH_3]^+$. ^{1}H NMR ($CDCl_3$, 400 MHz): δ 8.20 (d, *J* = 2.0 Hz, 2H, C_6H_2), 7.87 (s, 2H, C*H*=N), 7.56 (d, *J* = 8.0 Hz, 2H, C_6H_2), 7.43 (m, 4H, aryl*H*), 7.31 (d, 4H, aryl*H*), 7.10 (m, H, aryl*H*), 6.99 (d, *J* = 8.4 Hz, 2H, aryl*H*), 6.35 (s, 2H, C*H*=N), 2.20 (s, 6H, CH_3), -0.74 (s, 6H, Al-CH_3), –0.75 (s, 6H, Al-CH_3).

Synthesis of $\{(Me_2Al)[2\text{-}(O)\text{-}5\text{-}(t\text{Bu})C_6H_2\text{-}1,3\text{-}(CH)_2][O(2\text{-}C_6H_4)_2N)_2]\}_2$ (**2**)

As for **1**, but using $[2,2'\text{-}O(C_6H_4N)_2\text{-}2,6\text{-}(4\text{-}t\text{-}BuC_6H_3OH)]_2$ (0.50 g, 0.68 mmol) and $AlMe_3$ (0.84 ml, 1.35 mmol) affording **2** as a yellow solid. Yield: 0.32 g, 55.2 %. Elemental analysis calculated for $C_{52}H_{54}N_4O_4Al_2$: C 73.23, H 6.38, N 6.57 %; found: C 72.97, H 5.96, N 6.95 %. IR (cm^{-1}): 3434 (s), 3069 (w), 2958 (m), 2927 (m), 2868 (w), 1623 (s), 1596 (s), 1582 (s), 1545 (s), 1484 (s), 1449 (s), 1391 (w), 1375 (m), 1364 (m), 1328 (w), 1304 (w), 1275 (m), 1242 (s), 1226 (s), 1182 (s), 1111(m), 1040 (w), 1016(w), 997 (w), 978 (w), 959 (w), 933 (w), 890 (w), 874 (w), 874 (w), 858 (w), 839 (w), 820 (w), 792 (m), 773 (s), 749 (w), 713 (m), 680 (m), 662 (m), 601(w), 550 (w). MS (E.I.): 853.5 $[M]^+$. ^{1}H NMR ($CDCl_3$, 400 MHz) δ 8.35 (d, *J* = 2.0 Hz, 2H, C_6H_2), 8.02 (s, 2H, C*H*=N), 7.62 (s, 2H, C*H*=N), 7.50 (d, 2H, *J* = 8.4 Hz, aryl*H*), 7.41 - 7.46 (m, 2H, aryl*H*), 7.26 - 7.30 (t, 4H, aryl*H*), 7.11-7.16 (m, 2H, aryl*H*), 7.04 - 7.08 (m, aryl*H*), 6.99 (dd, 2H, J_1 = 7.6 Hz, J_2 = 1.6 Hz, aryl*H*), 6.92 (dd, 2H, J_1 = 8.0 Hz, J_2 = 1.2 Hz, aryl*H*), 6.70 - 6.71 (d, 2H, *J* = 2.8 Hz, C_6H_2), 1.26 (s, 18H, $(CH_3)_3$), –0.83 (s, 6H, Al-CH_3), –0.84 (s, 6H, Al-CH_3).

Synthesis of $\{(Me_2Al)[2\text{-}(O)\text{-}5\text{-}(Cl)C_6H_2\text{-}1,3\text{-}(CH)_2][O(2\text{-}C_6H_4)_2N)_2]\}_2$ (**3)**

As for **1**, but using $[2,2'\text{-}O(C_6H_4N)_2\text{-}2,6\text{-}(4\text{-}Cl\text{-}C_6H_3OH)]_2$ (0.50 g, 0.72 mmol) and $AlMe_3$ (0.90 ml, 1.43 mmol) affording **3** as a yellow solid. Yield: 0.36 g, 61.8 %. Elemental analysis calculated for $C_{44}H_{36}N_4O_4Cl_2Al_2$: C 65.28, H 4.48, N 6.92 %; found: C 64.81, H 4.50, N 6.95 %. IR (cm^{-1}): 3409 (s),

3064 (m), 2962 (m), 2930 (m), 2872 (m), 1610 (s), 1577 (s), 1550 (m), 1502 (s), 1487 (s), 1449 (s), 1374 (m), 1328 (m), 1261 (s) , 1235 (s), 1212 (s), 1158 (s), 1105 (m), 1045 (m), 930 (w), 866 (w), 800 (w), 744 (s), 694 (w), 620(w), 465(w). MS (E.I.): 831.0 $[M+Na]^+$. ^{1}H NMR ($CDCl_3$, 400 MHz): δ 8.34 (d, *J* = 2.8 Hz, 2H, C_6H_2), 7.97 (s, 2H, C*H*=N), 6.97-7.58 (m, 18H, aryl*H*), 6.59 (d, *J* = 2.8, 2H, C*H*=N) -0.67 (s, 6H, Al-CH_3), -0.73 (s, 6H, Al-CH_3).

Synthesis of $\{(Et_2Al)[2\text{-}(O)\text{-}5\text{-}(Me)C_6H_2\text{-}1,3\text{-}(CH)_2][O(2\text{-}C_6H_4)_2N)_2]\}_2$ (**4**)

To the ligand $[2,2^{/}\text{-}O(C_6H_4N)_2\text{-}2,6\text{-}(4\text{-}MeC_6H_3OH)]_2$ (0.50 g, 0.76 mmol) in hexane was added two equivalents of $AlEt_3$ (0.76 ml, 1.52 mmol) affording **4** as a yellow solid (yield 0.39 g, 62.3 %). Elemental analysis calculated for $C_{50}H_{50}N_4O_4Al_2$: C 72.80, H 6.11, N 6.79 %; found: C 72.45, H 5.98, N 6.95 %. IR (KBr) cm^{-1}: 3434 (s), 3067 (w), 2925 (w), 2891 (w), 2855 (w), 1793 (w), 1734 (w), 1625 (s), 1595 (s), 1552 (s), 1485 (s), 1452 (s), 1383 (s), 1333 (w), 1304 (w), 1273 (m), 1233 (s), 1217 (m), 1192 (m), 1163 (w), 1111 (m), 1043 (w), 990 (m), 946 (w), 932 (w), 877 (w), 859 (w), 832 (w), 791 (w), 754 (m), 742 (m), 670 (w), 647 (w), 612 (m), 565 (w), 545 (w), 454 (w), 419 (w). MS (E.I.): 849.8 $[M+Na]^+$. ^{1}H NMR ($CDCl_3$, 400 MHz) δ 8.16 (d, 2H, *J* = 4.8 Hz, C_6H_2), 7.91 (s, 2H, C*H*=N), 7.57 (d, *J* = 8.0 Hz, 2H, aryl*H*), 7.52 (s, 2H, C*H*=N), 7.43 - 7.48 (m, 2H, aryl*H*), 7.34 (m, 4H, aryl*H*), 7.06 - 7.13 (m, 6H, aryl*H*), 6.39 (dd, *J* = 8.0 Hz, *J* = 1.6 Hz, 2H, aryl*H*), 6.39 (d, 2H, *J* = 2.4Hz, C_6H_2), 2.19 (s, 6H, CH_3), 0.94 (t, *J* = 8.0 Hz, 6H, Al-CH_2CH_3), 0.74 (t, *J* = 8.4 Hz, 6H, Al-CH_2CH_3), –0.07 - –0.09 (overlapping m, 8H, Al-CH_2CH_3).

Synthesis of $\{(Et_2Al)[2\text{-}(O)\text{-}5\text{-}(t\text{Bu})C_6H_2\text{-}1,3\text{-}(CH)_2][O(2\text{-}C_6H_4)_2N)_2]\}_2$ (**5**)

To the ligand $[2,2^{/}\text{-}O(C_6H_4N)_2\text{-}2,6\text{-}(4\text{-}t\text{-}BuC_6H_3OH)]_2$ (0.50 g, 0.68 mmol) in hexane was added two equivalents of $AlEt_3$ (0.72 ml, 1.44 mmol) affording **5** as a yellow solid (yield 0.41 g, 66.4 %).

Elemental analysis calculated for $C_{56}H_{62}N_4O_4Al_2$: C 73.99, H 6.87, N 6.16 %; found: C 73.51, H 6.68, N 5.83 %. IR (KBr) cm^{-1}: 2929 (w), 2858 (w), 1621 (s), 1577 (m), 1545 (s), 1484 (s), 1447 (s), 1381 (w), 1320 (w), 1300 (w), 1244 (m), 1214 (m), 1182 (m), 1157 (m), 1110 (m), 1030 (m), 1014 (w), 983 (w), 937 (w), 870 (w), 856 (w), 838 (w), 810 (w), 792 (w), 752 (s), 705 (w), 668 (w), 649 (w), 602 (w), 476 (w). MS (E.I.): 863.55 $[M]^+$. ^1H NMR ($CDCl_3$, 400 MHz): δ 8.29 (d, J = 2.4 Hz, 2H, C_6H_2), 8.10 (s, 2H, C*H*=N), 7.73 (s, 2H, C*H*=N), 6.97 - 7.46 (m, 16H, aryl*H*), 6.06 (d, J = 2.8 Hz, C_6H_2), 0.94 (t, J = 8.0 Hz, 6H, Al-CH_2CH_3), 0.63 (t, J = 8.0 Hz, 6H, Al-CH_2CH_3), –0.06 - –0.22 (overlapping m, 8H, Al-CH_2CH_3).

Synthesis of $\{(Et_2Al)[2\text{-}(O)\text{-}5\text{-}(Cl)C_6H_2\text{-}1,3\text{-}(CH)_2][O(2\text{-}C_6H_4)_2N)_2]\}_2$ (**6**)

To the ligand $[2,2'\text{-}O(C_6H_4N)_2\text{-}2,6\text{-}(4\text{-}Cl\text{-}C_6H_3OH)]_2$ (0.50 g, 0.72 mmol) in hexane was added two equivalents of $AlEt_3$ (0.72 ml, 1.44 mmol) affording **6** as a yellow solid. Yield: 0.42 g, 67.5 %. Elemental analysis calculated for $C_{48}H_{44}N_4O_4Cl_2Al_2$: C 66.59, H 5.12, N 6.47 %; found: C 66.15, H 5.35, N 6.21 %. IR (KBr): cm^{-1} 2929 (w), 2858 (w), 1621 (s), 1577 (m), 1545 (s), 1484 (s), 1447 (s), 1381 (w), 1320 (w), 1300 (w), 1244 (m), 1214 (m), 1182 (m), 1157 (m), 1110 (m), 1030 (m), 1014 (w), 983 (w), 937 (w), 870 (w), 856 (w), 838 (w), 810 (w), 792 (w), 752 (s), 705 (w), 668 (w), 649 (w), 602 (w), 476 (w). MS (E.I.): 863.55 $[M]^+$. ^1H NMR ($CDCl_3$, 400 MHz): δ 8.29 (d, J = 2.4 Hz, 2H, C_6H_2), 8.02 (s, 2H, C*H*=N), 7.02 - 7.73 (m, 18H, aryl*H*), 6.06 (d, J = 4.2 Hz, C_6H_2), 0.94 (t, J = 8.0 Hz, 6H, Al-CH_2CH_3), 0.73 (t, J = 8.0 Hz, 6H, Al-CH_2CH_3), –0.05 - –0.11 (overlapping m, 8H, Al-CH_2CH_3).

Synthesis of $\{(Me_2Al)(MeAl)[2\text{-}(O)\text{-}5\text{-}(t\text{Bu})C_6H_2\text{-}1,3\text{-}(CH)_2][(CH_2CH_2)(2\text{-}C_6H_4)_2N)_2]_2\}\cdot 2^1/_4MeCN$ (**7**$\cdot 2^1/_4$MeCN)

To the ligand [2,2′-$CH_2CH_2(C_6H_4N)_2$-2,6-(4-*t*$BuC_6H_3OH)]_2$ (0.50 g, 0.65 mmol) in toluene was added two equivalents of $AlMe_3$ (0.69 ml, 2M solution in toluene, 1.38 mmol), and the system was refluxed for 12 h. Following removal of volatiles *in-vacuo*, the residue was extracted in MeCN (30 cm^3), and on prolonged standing at room temperature afforded small orange crystals of **7**·$2^1/_4$MeCN. Yield: 0.13 g, 24 %. Elemental analysis calculated for $C_{59.5}H_{66.75}N_{6.25}O_2Al_2$: C 74.80, H 7.04, N 9.16 %; found: C 74.59, H 6.84, N 9.08 %. IR (KBr) cm^{-1}: 3646 (w), 1650 (w), 1590 (m), 1261 (s), 1234 (m), 1199 (m), 1149 (m), 1107 (bs), 1005 (s), 922 (w), 904 (w), 881 (m), 797 (s), 753 (m), 635 (m).

Synthesis of $\{(Et_2Al)[2\text{-}(O)\text{-}5\text{-}(Me)C_6H_2\text{-}1,3\text{-}(CH)_2][(CH_2CH_2)(2\text{-}C_6H_4)_2N)_2]\}_2$ (**8**)

To the ligand [2,2′-$CH_2CH_2(C_6H_4N)_2$-2,6-(4-$MeC_6H_3OH)]_2$ (0.50 g, 0.74 mmol) in toluene was added two equivalents of $AlEt_3$ (0.73 ml, 1.47 mmol), and the system was refluxed for 12 h. Following removal of volatiles *in-vacuo*, the residue was extracted in MeCN (30 cm^3), and on prolonged standing at room temperature afforded small yellow crystals of **8**. Yield: 0.35 g, 55.8 %. Elemental analysis calculated for $C_{54}H_{58}N_4O_2Al_2$: C 76.39, H 6.88, N 6.60 %; found: C 76.59, H 6.44, N 7.08 %. IR (KBr) cm^{-1}: 1626 (m), 1592 (w), 1556 (m), 1339 (w), 1261 (s), 1240 (w), 1210 (w), 1191 (w), 1177 (w), 1157 (w), 1094 (s), 1019 (s), 947 (w), 918 (w), 870 (w), 800 (s), 769 (m), 749 (m), 740 (w), 727 (m), 694 (w), 671 (w), 646 (w), 628 (w). MS (MALDI-ToF): 764 (M^+ – 2Et – Al). ^{1}H NMR ($CDCl_3$, 400 MHz): δ 8.24 (s, 2H, C*H*=N), 8.17 (d, 2H, *J* = 2.0 Hz, C_6H_2), 7.60 (d, *J* = 7.60 Hz, 2H, aryl*H*), 7.40 (t, 2H, *J* = 7.2 Hz, aryl*H*), 7.26 (t, 4H, *J* = 6.0 Hz, aryl*H*), 6.99 (d, 2H, *J* = 5.6 Hz, aryl*H*), 6.90 (t, 2H, *J* = 7.2 Hz, aryl*H*), 6.81 (d, 2H, *J* = 7.6 Hz, aryl*H*), 6.68 (d, 2H, *J* = 2.4 Hz, C_6H_2), 6.62 (d, 2H, *J* = 6.8 Hz, aryl*H*), 6.42 (s, 2H, C*H*=N), 3.81 (dt, J_1 = 12.8 Hz, J_2 = 4.0 Hz, 2H, CH_2), 3.69 (td, J_1 = 13.2 Hz, J_2 = 4.0 Hz, 2H, CH_2), 3.01 (dt, J_1 = 14.0 Hz, J_2 = 4.8 Hz, 2H, CH_2), 2.68 (td, J_1 = 12.8 Hz, J_2 = 4.4 Hz,

2H, CH_2), 2.41 (s, 6H, CH_3), 0.94 (t, 6H, *J* = 8.4 Hz, Al-CH_2CH_3), 0.72 (t, 6H, *J* = 8.0 Hz, Al-CH_2CH_3), 0.05 (m, 4H, Al-CH_2), 0.32 (m, 4H, Al-CH_2).

Synthesis of [Al(**L**^{3})(**L**^{3}H)]·4toluene (**9**·4toluene)

To the ligand [2,2$^/$-O(C_6H_4N)$_2$-2,6-(4-ClC_6H_3OH)]$_2$ (0.50 g, 0.72 mmol) in hexane (30 ml) was added $AlEt_3$ (0.20 ml, 1.9 M, 0.38 mmol), and the system was refluxed for 12 h. Following removal of volatiles *in-vacuo*, the residue was extracted in MeCN (30 cm^3), and on prolonged standing at room temperature afforded small yellow/orange crystals of **9**·4toluene. Yield: 0.24 g, 48 %. Elemental analysis calculated for $C_{80}H_{50}N_8O_8Cl_4Al$: C 67.67, H 3.55, N 7.89 %; found (sample dried *in vacuo* for 12 h): C 66.59*, H 3.74, N 7.38 %. *Despite repeated analyses, this was the best result for %C. IR (KBr) cm^{-1}: 2360 (m), 2341 (m), 1716 (w), 1616 (w), 1576 (w), 1540 (m), 1301 (m), 1260 (s), 1208 (w), 1093 (s), 1020 (s), 867 (m), 800 (s), 722 (m), 688 (w), 467 (w). MS (Positive ion nanospray): 1278.3 (M^+ – 4Cl); (MALDI-ToF, no matrix): 722.5 (M+ – **L**^{3}H$_2$). ^{1}H NMR ($CDCl_3$, 400 MHz): δ 8.90 (bs, 4H, C*H*=N), 8.50 (s, 2H, C*H*=N), 8.32 (s, 2H, C*H*=N), 7.61 (s, 4H, Ar-*H*), 7.25 - 7.12 (m, 28H, Ar-*H*), 7.02 (overlapping m, 10H, Ar-*H*).

Synthesis of [Al(**L**^{5})(**L**^{5}H)]·5MeCN (**10**·5MeCN)

To the ligand [2,2$^/$-CH_2CH_2(C_6H_4N)$_2$-2,6-(4-*t*BuC_6H_3OH)]$_2$ (0.50 g, 0.65 mmol) in hexane (30 ml) was added $AlEt_3$ (0.20 ml, 1.9 M, 0.38 mmol), and the system was refluxed for 12 h. Following removal of volatiles *in-vacuo*, the residue was extracted in MeCN (30 cm^3), and on prolonged standing at room temperature afforded small yellow crystals of **10**·5MeCN. Yield: 0.19 g, 37 %. Elemental analysis calculated for $C_{112}H_{113}N_{12}O_4Al$: C 78.30, H 6.63, N 9.78 %; found (sample dried *in vacuo* for 12 h): C 77.89, H 6.44, N 9.48 %. IR (KBr) cm^{-1}: 1630 (s), 1588 (m), 1573 (s), 1307 (m), 1262 (s), 1206 (m),

1155 (m), 1089 (s), 1034 (s), 1018 (s), 880 (w), 861 (w), 801 (m), 770 (w), 753 (m), 722 (s), 647 (w), 636 (w), 613 (w), 596 (w), 566 (w), 530 (w), 506 (w), 464 (w). MS (MALDI-ToF, no matrix): 790 (M^+ – LH). ^{1}H NMR ($CDCl_3$, 400 MHz): δ 8.83 (bs, 2H, C*H*=N), 8.71 (bs, 2H, C*H*=N), 8.35 (bs, 4H, C*H*=N), 8.29 (m, 2H, aryl*H*), 7.91 – 6.18 (overlapping m, 32 H, aryl*H*), 5.88 (d, 2H, aryl*H*), 5.86 (d, 2H, J = 18.0 Hz, aryl*H*), 5.62 (d, 2H, J = 14.4 Hz, aryl*H*), 5.34 (bm, 2H, CH_2), 4.56 (bm, 2H, CH_2), 3.86 (bm, 2H, CH_2), 3.74 (bm, 2H, CH_2), 3.30 (bm, 2H, CH_2), 3.13 (overlapping m, 2H, CH_2), 3.07 (bm, 2H, CH_2), 2.91 (bm, 2H, CH_2), 2.44 (s, 3H, *Me*CN), 2.01 (s, 3H, *Me*CN), 0.92 (s, 6H, *Me*CN), 1.56 (s, 9H, C(CH_3)$_3$), 1.41 (s, 9H, C(CH_3)$_3$), 1.29 (s, 9H, C(CH_3)$_3$), 1.19 (s, 9H, C(CH_3)$_3$).

Synthesis of {(Me_2Al)$_2$[2-(O)-5-(*t*Bu)C_6H_2-1-(CH)-3-(C(Me)H][(O)(2-(N)-2′-C_6H_4N)$_2$]}$_2$·1.75toluene·1.25hexane (**11**·1.75toluene·1.25hexane)

As for **1**, but using [2,2′-O(C_6H_4N)$_2$-2,6-(4-*t*-BuC_6H_3OH)]$_2$ (0.50 g, 0.68 mmol) and $AlMe_3$ (1.7 ml, 2.70 mmol) and then recrystallisation from a saturated hexane/toluene (50:50) solution at 0 ^{o}C afforded **11**·1.75toluene·1.25hexane as a red crystalline solid on prolonged standing at 0 ^{o}C (1 - 2 days). Yield 0.25 g, 36.9 %. Elemental analysis calculated for $C_{58}H_{72}N_4O_4Al_4$: C 69.87, H 7.28, N 5.62 %; found (sample dried *in vacuo* for 12 h): C 69.52, H 6.93, N 5.22 %. IR (cm^{-1}): 3413 (s), 3064 (m), 2929 (m), 2857 (m) 1624 (s), 1608 (s), 1551 (m), 1508 (s), 1486 (s), 1456 (s), 1377 (w), 1329 (m), 1261 (s), 1233 (m), 1192 (m), 1157 (w), 1101 (s), 1024 (s), 863 (m), 801 (w), 741 (m), 660 (w). MS (E.I.): 1017.43 $[M+Na]^+$. ^{1}H NMR ($CDCl_3$, 400 MH_Z): δ 8.29 (d, *J* = 2.4 Hz, 2H, C_6H_2), 8.02 (s, 2H, C*H*=N), 7.02 - 7.73 (m, 16H, aryl*H*), 6.06 (d, 2H, *J* = 4.2 Hz, C_6H_2), 4.55 (m, 1H, C*H*CH_3), 4.28 (m, 1H, C*H*CH_3), 1.66 (d, 3H, CH_3CH), 1.53 (d, 3H, CH_3CH), 1.25 (s, 9H, C(CH_3)$_3$), 0.89 (s, 9H, C(CH_3)$_3$), –0.52 (2× s, 6H, Al-CH_3), –0.77 (s, 3H, Al-CH_3), –0.87 (s, 3H, Al-CH_3), –0.89 (s, 3H, Al-CH_3), –1.14 (s, 3H, Al-CH_3), –1.37 (s, 3H, Al-CH_3), –1.39 (s, 3H, Al-CH_3).

Synthesis of $\{(Me_2Al)_2[2\text{-}(O)\text{-}5\text{-}(Cl)C_6H_2\text{-}1\text{-}(CH)\text{-}3\text{-}(C(Me)H][(O)(2\text{-}(N)\text{-}2'\text{-}C_6H_4N)_2]\}_2$ (**12**)

As for **9**, but using $[2,2'\text{-}O(C_6H_4N)_2\text{-}2,6\text{-}(4\text{-}Cl\text{-}C_6H_3OH)]_2$ (0.50 g, 0.72 mmol) and $AlMe_3$ (1.8 ml, 2.87 mmol), affording **12** as a red crystalline solid on prolonged standing at ambient temperature (1 - 2 days). Yield: 0.30 g, 43.8 %. Elemental analysis calculated for $C_{50}H_{54}N_4O_4Cl_2Al_4$: C 62.96, H 5.71, N 5.87 %; found: C 62.39, H 5.47, N 5.96 %. IR (cm^{-1})： 3434 (s), 3061 (w) , 2928 (w), 1619 (s), 1597 (m), 1576 (m), 1543 (s), 1447 (s), 1384 (m), 1321 (m), 1301 (w), 1246 (s), 1212 (s), 1183 (m), 1160 (w), 1104 (s), 1031 (s), 940 (w)， 868 (w), 839 (w), 810 (m), 753 (m), 709 (w), 699 (m), 685 (w), 636 (w), 579 (w), 447 (w), 529 (w), 476(w). MS (E.I.): 917.18 $[M - Cl]^+$. ^1H NMR ($CDCl_3$, 400 MHz): δ 8.07 (s, 2H, C*H*=N), 7.43 (td, 2H, J_1 = 8.4 Hz, J_2 = 1.6 Hz, aryl*H*), 7.36 (m, 2H, *aryl*H), 7.32 (dd, 2H, J_1 = 7.2 Hz, J_2 = 1.6 Hz, aryl*H*), 7.27 (d, 2H, *J* = 2.8 Hz, C_6H_2), 7.18 (m, 2H, aryl*H*), 7.08 (td, 2H, J_1 = 8.4 Hz, J_2 = 1.6 Hz, aryl*H*), 6.99 (d, 2H, *J* = 7.6 Hz, aryl*H*), 6.71 (d, 2H, *J* = 2.4 Hz, C_6H_2), 6.52 (m, 4H, aryl*H*), 4.47 (q, 2H, *J* = 7.2 Hz, C*H*CH_3), 1.59 (d, 6H, *J* = 7.2 Hz, CHC*H*$_3$), –0.49 (s, 6H, Al-C*H*$_3$), –0.73 (s, 6H, Al-C*H*$_3$), –0.83 (s, 6H, Al-C*H*$_3$), –1.01 (s, 6H, Al-C*H*$_3$).

Synthesis of $\{(Et_2Al)_2[2\text{-}(O)\text{-}5\text{-}(Me)C_6H_2\text{-}1\text{-}(CH)\text{-}3\text{-}(C(Et)H][(O)(2\text{-}(N)\text{-}2'\text{-}C_6H_4N)_2]\}_2$ (**13**)

As for **9**, but using $[2,2'\text{-}O(C_6H_4N)_2\text{-}2,6\text{-}(4\text{-}MeC_6H_3OH)]_2$ (0.50 g, 0.76 mmol) $AlEt_3$ (1.5 ml, 2M, 3.04 mmol), affording **13** as a purple solid on prolonged standing at ambient temperature (1 - 2 days). Yield: 0.24 g, 30 %. Elemental analysis calculated for $C_{62}H_{80}N_4O_4Al_4 \cdot 4$toluene: C 76.03, H 7.94, N 3.94 %; found: C 76.47, H 7.61, N 4.09 %. IR (cm^{-1}): 3413 (s), 3064 (m), 2929 (m), 2857 (m) 1624 (s), 1608 (s), 1551 (m), 1508 (s), 1486 (s), 1456 (s), 1377 (w), 1329 (m), 1261 (s), 1233 (m), 1192 (m), 1157 (w), 1101 (s), 1024 (s), 863 (m), 801 (w), 741 (m), 660 (w). MS (E.I.): 1421.8 $[M + 4toluene]^+$, 995.4 $[M - 2Et]^+$, 966.4 $[M - 3Et]^+$, 937.4 $[M - 4Et]^+$. ^1H NMR ($CDCl_3$, 400 MHz): δ 7.99 (s, 2H, aryl*H*),

7.49 (dd, 2H, J_1=7.6 Hz, J_2=1.2 Hz, aryl*H*), 7.46 (dd, 2H, *J*=1.2 Hz, C_6H_2), 7.35 (td, 2H, J_1=7.6, J_2 =2.0 Hz, aryl*H*), 7.16 (td, 2H, J_1=7.6 Hz, J_2 =2.0 Hz, aryl*H*), 7.07 (dd, 2H, J_1=8.0 Hz, J_2=2.0 Hz, aryl*H*), 7.02 - 7.05 (m, 4H, aryl*H*), 6.96 (dd, 2H, J_1=8.0 Hz, J_2=2.0 Hz, aryl*H*), 6.93 (dd, 2H, J_1=8.0 Hz, J_2=2.0 Hz, aryl*H*), 6.85 (td, 2H, J_1=8.4 Hz, J_2=2.0 Hz, aryl*H*), 6.68 (td, 2H, J_1=8.4 Hz, J_2=2.0 Hz, aryl*H*), 6.62 (td, 2H, J_1=8.4 Hz, J_2=1.2 Hz, aryl*H*), 6.75 (dd, 2H, J_1=8.4 Hz, J_2=1.2 Hz, aryl*H*), 6.61 (dd, 2H, J_1=8.4 Hz, J_2=1.2 Hz, aryl*H*), 6.53 (m, 4H, aryl*H*), 6.20 (td, 2H, J_1=8.4 Hz, J_2 =1.2 Hz, aryl*H*), 6.14 (d, 2H, *J*=13.2 Hz, C_6H_2) (the aromatic region is a combination of 4 toluene + **13**), 5.61 (s, 2H, C*H*=N), 4.55 (m, 2H, *NCH*Et), 2.26 (m, 2H, CHCH_2CH$_3$), 2.17 (m, 2H, CH_2CH$_3$), 1.91 (s, 6H, CH$_3$ toluene), 1.84 (s, 6H, CH$_3$ toluene), 1.63 (m, 6H, CH$_3$), 1.49 (m, 2H, AlCH_2CH$_3$), 1.42 (m, 2H, AlCH_2CH$_3$), 0.94 (overlapping m, 12H, CHCH$_2$CH$_3$ + Al-CH$_2$CH_3), 0.78 (t, *J* = 8.4 Hz, 6H, Al-CH$_2$CH_3), 0.53 (t, *J* = 7.2 Hz, 6H, Al-CH$_2$CH_3), 0.42 (t, *J* =8.2 Hz, 6H, Al-CH$_2$CH_3), –0.05 (m, 4H, Al-CH_2CH$_3$), –0.26 (m, 4H, Al-CH_2CH$_3$), –1.21 (m, 2H, Al-CH_2CH$_3$) and –1.50 (m, 2H, Al-CH_2CH$_3$).

Synthesis of {(Et$_2$Al)$_2$[2-(O)-5-(Cl)C$_6$H$_2$-1-(CH)-3-(C(Et)H][(O)(2-(N)-2$^{/}$-C$_6$H$_4$N)$_2$]}$_2$ (**14**)

As for **9**, but using [2,2$^{/}$-O(C$_6$H$_4$N)$_2$-2,6-(4-Cl-C$_6$H$_3$OH)]$_2$ (0.50 g, 0.72 mmol) and AlEt$_3$ (1.44 ml, 2M, 2.88 mmol) affording **14** as a purple solid on prolonged standing at ambient temperature (1 - 2 days). Yield 0.43 g, 54 %. Elemental analysis calculated for $C_{60}H_{74}N_4O_4Cl_2Al_4$: C 65.87, H 6.82, N 5.12 %; found: C 65.47, H 6.63, N 4.94 %. MS (E.I.): 1116.4 $[M+Na]^+$. IR (cm^{-1}): 1618 (w), 1551 (w), 1304 (m), 1261 (s), 1208 (w), 1153 (w), 1096 (s), 1020 (s), 918 (w), 890 (w), 801 (s), 722 (m), 660 (w), 619 (w), 467 (w). ^{1}H NMR (CDCl$_3$, 400 MHz) δ 8.54 (s, 2H, C$_6H_2$), 7.63 (dd, 2H, J_1=7.2 Hz, J_2=1.6 Hz, aryl*H*), 7.60 (s, 2H, aryl*H*), 7.49 (td, 2H, J_1=7.6 Hz, J_2 =1.6 Hz, aryl*H*), 7.41 (s, 2H, aryl*H*), 7.33 (dd, 2H, J_1=7.6 Hz, J_2=1.6 Hz, aryl*H*), 7.26 - 7.31 (m, 4H, aryl*H*), 7.22 (td, 2H, J_1=9.2 Hz, J_2=1.6 Hz, aryl*H*), 7.16 (m, 2H, J_1=9.2 Hz, J_2=1.6 Hz, aryl*H*), 7.09 (dd, 2H, J_1=8.0 Hz, J_2=1.6 Hz, aryl*H*), 7.00

(td, 2H, J_1=8.4, J_2=1.2 Hz, aryl*H*), 6.95 (2x s, 2H, *J*=2.8 Hz, aryl*H*), 6.82 (td, 2H, J_1=8.4, J_2=1.2 Hz, aryl*H*), 6.75 (dd, 2H, J_1=8.4 Hz, J_2=1.2 Hz, aryl*H*), 6.61 (dd, 2H, J_1=8.4, J_2=1.2 Hz, aryl*H*), 6.33 (dd, 2H, J_1=8.8 Hz, J_2=1.2 Hz, aryl*H*) (these peaks are a combination of 2.8toluene plus **14**), 6.14 (s, 2H, C*H*=N), 4.60 (m, 2H, J_1=9.6, J_2=1.4 Hz, C*H*Et), 2.36 (m, 2H, CHCH_2CH$_3$), 2.20 (m, 2H, CHCH_2CH$_3$), 2.10 (s, 8.4H, CH$_3$ of 2.8toluene), 1.77 (m, 2H, Al-CH_2CH$_3$), 1.65 (m, 2H, Al-CH_2CH$_3$), 1.02 (overlapping m, *J* = 8.0 Hz, 12H, CHCH$_2$CH_3 + Al-CH$_2$CH_3), 0.86 (t, *J* = 7.2 Hz, 6H, Al-CH$_2$CH_3), 0.74 (t, *J* = 8.2 Hz, 6H, Al-CH$_2$CH_3), 0.52 (t, *J* = 8.2 Hz, 6H, Al-CH$_2$CH_3), 0.04 (m, 4H, Al-CH_2CH$_3$), –0.14 (m, 4H, Al-CH_2CH$_3$), –1.13 (m, 2H, Al-CH_2CH$_3$), –1.41 (m, 2H, Al-CH_2CH$_3$).

Description of emission studies

The Photoluminescence emission spectra were collected in a quartz cuvette (10 × 10 mm), using a PerkinElmer LS55 spectrophotometer with an excitation slit width of 10 nm and an emission slit width set at 5 nm. The excitation wavelength was fixed at 400 nm. The emission spectra were corrected using the solvent emission as background. The measurements were performed at standard pressure and room temperature.

ROP procedure

ε-Caprolactone: Typical polymerization procedures in the presence of one equivalent of benzyl alcohol (Table 4, run 1) are as follows. A toluene solution of **2** (0.010 mmol, in 1.0 mL toluene) and BnOH (0.010 mmol) were added into a Schlenk tube in the glove-box at room temperature. The solution was stirred for 2 min, and then ε-caprolactone (2.5 mmol) along with 1.5 mL toluene was added to the solution. The reaction mixture was then placed into an oil bath pre-heated to the required temperature, and the solution was stirred for the prescribed time. The polymerization mixture was then quenched by

addition of an excess of glacial acetic acid (0.2 mL) into the solution, and the resultant solution was then poured into methanol (200 mL). The resultant polymer was then collected on filter paper and was dried *in* vacuo.

rac-Lactide: 5 mL of dry toluene were transferred into a Schlenk tube containing the desired amount of catalyst. The solution was stirred and maintained at the polymerization temperature with the aid of an oil bath. Benzyl alcohol was then added from a 0.6 M solution in toluene. After an additional five minutes, the polymerization was started by the addition of 1.0 mL of *rac*-lactide.

Crystallography

Diffraction data for $\mathbf{L^1}H_2$·MeCN and $L^2(tosyl)_2$ were measured on Bruker SMART 1000 CCD and APEX 2 CCD diffractometers respectively, with Mo-Kα radiation, at 150(2) K using 0.3 ° ω-scans. [24] Corrections were made for absorption and for Lorentz and Lp effects. [25] The structures were solved by direct methods and refined on F^2 by full-matrix-least squares. [26]

For the remaining samples, diffraction intensities were measured on Oxford Diffraction Xcalibur-3 or New Gemini CCD diffractometers equipped with Mo-Kα radiation and graphite monochromator. The data for $\mathbf{L^2}H_2$·2(acetone) were recorded at room temperature but the other samples were measured at temperatures between 120 and 140 K. Intensity data were measured by thin-slice ω- and φ-scans. Data were processed using the CrysAlis-CCD and -RED [27] programs. The structures were determined by the direct methods routines in the SHELXS program [28] and refined by full-matrix least-squares methods, on F^2, in SHELXL. [29]

For $\mathbf{7}\cdot2^1/_4$MeCN, data collected at Daresbury Laboratory Station 9.8. [30] The crystal was weakly diffracting, so data was only integrated to $2\theta = 45°$. The *t*Bu group at C89 was modeled as two-fold

disordered with a major component of 72.8(9)%, whilst the MeCN containing N12 was refined at half weight. For **8**, data were collected using an Agilent Xcalibur diffractometer with an Eos detector. Single crystal diffraction data for **9**·4toluene and **10**·5MeCN were collected by the UK National Crystallography Service using a Rigaku FR-E+ diffractometer. This operates with a SuperBright rotating anode X-ray generator and high flux optics. For **10**·5MeCN, one MeCN was refined as point atoms, the other four as regions of diffuse electron density using the Platon Squeeze procedure [16]. Squeeze identifies 2 voids per unit cell, each containing 207 electrons. Inspection of the residual electron density prior to squeeze strongly suggested 4 MeCNs. Each MeCN contains 22 electrons so, although 207 electrons indicates *ca*. 9.4 MeCNs, only 8 were added per void, or 4 per metal complex. For **11**·1¾toluene·$1^{1}/_{4}$hexane, data were collected with an Agilent Gemini diffractometer using molybdenum radiation and an Eos S2 detector. Disordered solvent was modelled using the Squeeze routine, which identified two voids per unit cell containing a total of 1210 electrons. This was modelled using 9 toluene and 4 hexane molecules (the ratio of disordered toluene to hexane cannot be estimated by this technique).

Structures were solved using Direct Methods implemented within SHELXS-2013 and refined within SHELXL-2014. [31-33] Further details are provided in Table 5.

CCDC 1442772 – 1442778 (Schiff-base pro-ligands) and 1463685 – 1463689 (organoaluminium complexes) contain the supplementary crystallographic data for this paper. These data can be obtained free of charge from The Cambridge Crystallographic Data Centre via www.ccdc.cam.ac.uk/data_request/cif.

Acknowledgements

Sichuan Normal University and the National Natural Science Foundation of China (grants 51273133 and 51443004) are thanked for financial support. The Special Funds for sharing large precision equipment (no. DJ2014-22) at Sichuan Normal University is also thanked. CR thanks the EPSRC for a travel grant (EP/L012804/1) and the National Crystallographic Service at the University of Southampton (for data collection of **9**·4toluene and **10**·5MeCN). The CCLRC is thanked for the award of beamtime (complex **7**·$2^1/_4$MeCN) at SRS Daresbury Laboratory (Station 9.8), and the EPSRC Mass Spectrometry Service at Swansea is thanked for data. TB is grateful to an Alan Katritzky Scholarship awarded by UEA.

Supporting Information Available: X-ray crystallographic files CIF format for the structure determinations of compound $\mathbf{L^1}H_2$·MeCN, $\mathbf{L^2}H_2$·MeCN, $\mathbf{L^2}H_2$·2(Me_2CO) and $\mathbf{L^2}H_2$·n(MeCOOEt), n=1 and 2, $\mathbf{L^2}H_2$·2(PhMe), $\mathbf{L^2}$(tosyl)$_2$, **7**·$2^1/_4$MeCN, **8**, **9**·4toluene, **10**·5MeCN and **11**·1¾toluene·$1^1/_4$hexane.

References

[1] (a) J. R. Askim, M. Mahmoudi and K. S. Suslick, *Chem. Soc. Rev*. **2013**, *42*, 8649. (b) Z. Guo, S. Park, J. Yoon and I. Shin, *Chem. Soc. Rev*. **2014**, *43*, 16.

[2] C. Reichardt and T. Welton, *Solvents and solvent effects in organic chemistry*, 4th Ed. Weinheim, Germany, Wiley-VCH, **2010**.

[3] (a) K. M. Mullen and P. D. Beer, *Chem. Soc. Rev*. **2009**, *38*, 1701.

[4] See for example, (a) E. M. Hodnet and J. W. Dunn, *J. Med. Chem*. **1970**, *13*, 768. (b) S. N. Pandeya, D. Sriram, G. Nath and E. De Clercq, *Il Farmaco* **1999**, *54*, 624. (c) A. H. El-Masry, H. H. Fahmy and S. H. Abdelwahed, *Molecules* **2000**, *5*, 1429. (c) A. A. Jarrahpour and M. Zarei, *Molbank* **2004**, M377. (e) H. L. Siddiqui, A. Iqbal, S. Ahmad and G. W. Weaver, *Molecules* **2006**, *11*, 206.

[5] (a) S. Brooker, *Coord. Chem. Rev*. **2001**, *222*, 33. (b) W. Radecka-Paryzek, V. Patroniak and J. Lisowski, *Coord. Chem. Rev*. **2005**, *249*, 2156.

[6] (a) F. H. Allen, *Acta Crystallogr. Sect. B: Struct. Sci*., **2002**, *58*, 380. (b) W. Yang, K. -Q. Zhao, B. -Q. Wang, C. Redshaw, M. R. J. Elsegood, J. -L. Zhao and T. Yamato, *Dalton Trans*. **2016**, *45*, 226-236.

[7] (a) A. Arbaoui, C. Redshaw and D. L. Hughes, *Chem. Commun*. **2008**, 4717. (b) A. Arbaoui, C. Redshaw and D. L. Hughes, *Supramol. Chem*. **2009**, *21*, 35.

[8] F. Majoumo-Mbe, E. Smolensky, P. Lőnnecke, D. Shpasser, M. S. Eisen and E. Hey-Hawkins, *J. Mol. Catal. A: Chem*. **2005**, *240*, 91.

[9] R. Mazarro, I. Gracia, J. F. Rodriquez, G. Storti and M. Morbidelli, *Polym. Int*. **2012**, *61*, 265.

[10] P. Chakraborty, J. Adhikary, S. Samanta, I. Majumder, C. Massera, D. Escudero, S. Ghosh, A. Bauza, A. Frontera and D. Das, *Dalton Trans*. **2015**, *44*, 20032.

[11] Y. Wei, S. Wang and S. Zhou, *Dalton Trans*. **2016**, *45*, 4471.

[12] (a) S. R. Korupoju and P. S. Zacharias, *Chem. Commun*. **1998**, 1267. (b) S. J. Na, D. J. Joe, S. Sujith, W. -S. Han, S. O. Kang and B.Y. Lee, *J. Organomet. Chem*. **2006**, *691*, 611.

[13] (a) S. Brooker, G. S. Dunbar and T. Weyhermuller, *Supramol.Chem*. **2001**, *13*, 601. (b) J. Gao, J. H. Reibenspies, R. A. Zingaro, R. Woolley, A. E. Martell and A. Clearfield, *Inorg. Chem*. **2005**, *44*, 232. (c) S. J. Na, D. J. Joe, S. Sujith, W. -S. Han, O. S. Kang and B. Y. Lee, *J. Organomet. Chem*. **2006**, *691*, 611. (d) M. Paluch, J. Lisowski and T. Lis, *Dalton Trans*. **2006**, 381.

[14] (a) R. W. Stotz and R. C. Stoufer, *J. Chem. Soc. Chem. Commun*. **1970**, 1682. (b) J. D. O. Cabral, M. F. Cabral, M. G. B. Drew, F. S. Esho, O. Haas and S. M. Nelson, *J. Chem. Soc., Chem. Commun*.

1982, 1066. (c) T. W. Bell and F. Guzzo, *J. Chem. Soc., Chem. Commun*. **1986**, 769. (d) T. Sato, K. Sakai and T. Tsubomura, *Chem. Lett*. **1993**, 859. (e) S. W. A. Bligh, N. Cho, V. W. J. Cummins, E. G. Evagoroula, D. J. Kelly and M. McPartlin, *J. Chem. Soc., Dalton Trans*. **1994**, 3369. (f) D. A. Plattner, A. K. Beck and M. Neuburger, *Helv. Chim. Acta* **2002**, *85*, 4000. (g) M. Allmendinger, P. Zell, A. Amin, U. Thewalt, M. Klinga and B. Rieger, *Heterocycles* **2003**, *60*, 1065. (h) J. Gregolinski, J. Lisowski and T. Lis, *Org. Biomol. Chem*. **2005**, *3*, 3161.

[15] A. Arbaoui, C. Redshaw and D. L. Hughes, *Chem. Commun*. **2008**, 4717.

[16] A. L. Spek, *Acta Crystallogr*. **1990**, *A46*, C34.

[17] (a) J. M. Klerks, D. J. Stufkens, G. van koten and K. Vrieze, *J. Organomet Chem.* **1979**, *181*, 271. (b) V. C. Gibson, C. Redshaw, A. J. P. White and D. J. Williams, *J. Organomet Chem.* **1998**, *550*, 453. (c) M. Bruce, V. C. Gibson, C. Redshaw, G. A. Solan, A. J. P.White and D. J. Williams, *Chem. Commun*., **1998**, 2523. (d) V. C. Gibson, D. Nienhuis, C. Redshaw, A. J. P. White and D. J. Williams, *Dalton Trans.* **2004**, 1761. (e) V. C. Gibson, C. Redshaw, G. A. Solan, A. J. P. White and D. J. Williams, *Organometallics* **2007**, *26*, 5119. (f) A. Arbaoui, C. Redshaw and D. L. Hughes, *Supramol. Chem*. **2009**, *21*, 35. (g) W. Alkarekshi, A. P. Armitage, O. Boyron, C. J. Davies, M. Govere, A. Gregory, K. Singh and G. A. Solan, *Organometallics*, **2013**, *32*, 249-259.

[18] (a) M. Shen, W. Zhang, K. Nomura and W. -H. Sun, *Dalton Trans.* **2009**, 9000. (b) M. Shen, W. Huang, W. Zhang, X. Hao, W. -H. Sun and C. Redshaw, *Dalton Trans*. **2010**, *39*, 9912. (c) M. -C. Chang, W. –Y. Lu, H. -Y. Chang, Y. –C. Lai, M. Y. Chiang, H. –Y. Chen and H. –Y. Chen, *Inorg. Chem*. **2015**, *54*, 11292.

[19] (a) N. Iwasa, S. Katao, J. liu, M. Fujiki, Y. Furukawa and K. Nomura, *Organometallics* **2009**, *28*, 2179. (b) D. Li, Y. Peng, C. Geng, K. Liu and D. Kong, *Dalton Trans*. **2013**, *42*, 11295. (c) W. –L. Kong, Z. –Y. Chai and Z. –X. Wang, *Dalton Trans*. **2014**, *43*, 14470. (d) W. Zhang, Y. Wang, L. Wang, C. Redshaw and W. –H. Sun, *J. Organomet. Chem*. **2014**, *750*, 65.

[20] C. Redshaw, M. A. Rowan, L. Warford, D. M. Homden, A. Arbaoui, M. R. J. Elsegood, S. H. Dale, T. Yamato, C. Pérez-Casas, S. Matsui and S. Matsuura, *Chem. Eur. J*. **2007**, 13, 1090-1107.

[21] T.K. Sen, A. Mukherjee, A. Modak, S.K. Mandel and D. Koley, *Dalton Trans*. **2013**, *42*, 1893.

[22] (a) R. S. Drago, M. J. Desmond, B. B. Corden and K. A. Miller, *J. Am. Chem. Soc*. **1983**, *105*, 2295. (b) J. J. Randell, C. E. Lewis and P.M. Slagan, *J. Org. Chem*. **1962**, *27*, 4098.

[23] V. C. Gibson, C. Redshaw, W. Clegg, M. R. J. Elsegood, U. Siemeling and T. Türk, *Polyhedron* **2004**, *23*, 189.

[24] SMART and SAINT (**2001**) software for CCD diffractometers. Bruker AXS Inc., Madison, USA.

[25] G. M. Sheldrick, SHELXTL user manual, version 6.10. Bruker AXS Inc., Madison, WI, USA, (**2000**).

[26] G. M. Sheldrick, SHELX-97 − Programs for crystal structure determination (SHELXS) and refinement (SHELXL), *Acta Crystallogr*. **2008**, *A64*, 112-122.

[27] Programs CrysAlis-CCD and -RED, Oxford Diffraction Ltd., Abingdon, UK (**2005**).

[28] *'International Tables for X-ray Crystallography'*, Kluwer Academic Publishers, Dordrecht (**1992**). Vol. C, pp. 500, 219 and 193.

[29] L. J. Farrugia, *J. Appl. Cryst.* **2012**, *45*, 849–854.

[30] APEX 2 and SAINT (2007) software for CCD diffractometers. Bruker AXS Inc., Madison, USA.

[31] G. M. Sheldrick, *Acta Crystallogr*. **2008**, *64*, 112.

[32] G. M. Sheldrick, SHELXTL user manual, version 6.10. Bruker AXS Inc., Madison, WI, USA, (**2000**).

[33] G. M. Sheldrick, *Acta Cryst*. **2015**, *C71*, 3-8

Table 5. Crystallographic data for $\mathbf{L^1}H_2\cdot$MeCN, $\mathbf{L^2}H_2\cdot$MeCN, $\mathbf{L^2}H_2\cdot 2(Me_2CO)$ and $\mathbf{L^2}H_2\cdot$n(MeCOOEt), n=1 and 2, $\mathbf{L^2}H_2\cdot 2$(PhMe) and $\mathbf{L^2}$(tosyl)$_2$.

Compound	$\mathbf{L^1}H_2\cdot$MeCN	$\mathbf{L^2}H_2\cdot$MeCN	$\mathbf{L^2}H_2\cdot$MeCOOEt	$\mathbf{L^2}H_2\cdot 2$(MeCOOEt)	$\mathbf{L^2}H_2\cdot 2(Me_2CO)$	$\mathbf{L^2}H_2\cdot 2$(PhMe)	$\mathbf{L^2}$(tosyl)$_2$
Formula	$C_{42}H_{32}N_4O_4\cdot C_2H_3N$	$C_{48}H_{44}N_4O_4\cdot C_2H_3N$	$C_{48}H_{44}N_4O_4\cdot C_4H_8O_2$	$C_{48}H_{44}N_4O_4\cdot 2(C_4H_8O_2)$	$C_{48}H_{44}N_4O_4\cdot 2(C_3H_6O)$	$C_{48}H_{44}N_4O_4\cdot 2(C_7H_8)$	$C_{62}H_{56}N_4O_8S_2$
Formula weight	697.77	781.92	828.97	917.08	857.02	925.14	1049.23
Crystal system	Triclinic	Triclinic	Monoclinic	Monoclinic	Monoclinic	Monoclinic	Monoclinic
Space group	*P*$\bar{1}$	*P*$\bar{1}$	C2/c	C2/c	C2/c	$P2_1/n$	$P2_1/n$
Unit cell dimensions							
a (Å)	11.0841(6)	15.1737(5)	24.8335(10)	24.9034(15)	24.5582(10)	13.8127(5)	13.201(3)
b (Å)	12.2117(6)	15.3473(6)	11.2046(4)	11.5371(6)	12.1677(7)	16.8060(6)	13.348(3)
c (Å)	13.8841(7)	19.2180(7)	15.9714(11)	16.9261(12)	16.0892(7)	22.5196(9)	14.966(3)
α (°)	86.1299(8)	98.169(13)	90	90	90	90	90
β (°)	74.9778(8)	109.862(3)	101.497(6)	96.003(6)	98.942(4)	105.428(4)	94.913(3)
γ (°)	89.6361(8)	91.656(3)	90	90	90	90	90
V (Å^3)	1810.81(16)	4152.1(3)	4354.9(4)	4836.4(5)	4749.3(4)	5039.2(3)	2627.4(10)
Z	2	4	4	4	4	4	2
Temperature (K)	150(2)	140(2)	120.0(2)	120.0(2)	293(2)	130.0(1)	150(2)
Wavelength (Å)	0.71073	0.71073	0.71073	0.71073	0.71073	0.71073	0.71073
Calculated density (g.cm^{-3})	1.280	1.251	1.264	1.259	1.199	1.219	1.326
Absorption coefficient (mm^{-1})	0.08	0.08	0.083	0.084	0.078	0.076	0.164
Transmission factors (min./max.)	0.947, 0.979	0.942, 1.062	0.784, 1.000	0.799, 1.000	0.952,1.000	0.709, 1.000	0.960, 0.985
Crystal size (mm^3)	0.66 × 0.45 × 0.25	0.38 × 0.29 × 0.10	0.49 × 0.40 × 0.38	0.48 × 0.42 × 0.27	0.20 × 0.20 × 0.30	0.50 × 0.40 × 0.30	0.25 × 0.18 × 0.09
θ(max) (°)	29.0	22.5	27.5	25.0	25.0	25.0	23.0
Reflections measured	16012	33814	12474	12476	9158	27782	15869
Unique reflections	8329	10758	4880	4267	4173	8856	3661
R_{int}	0.013	0.086	0.031	0.032	0.018	0.055	0.044
Reflections with $F^2 > 2\sigma(F^2)$	6933	5230	3517	3777	3045	6118	2640
Number of parameters	487	1093	303	365	323	654	360
R_1 [$F^2 > 2\sigma(F^2)$]	0.050	0.043	0.049	0.117	0.047	0.059	0.047
wR_2 (all data)	0.141	0.083	0.130	0.253	0.133	0.154	0.143
GOOF, *S*	1.023	0.788	1.058	1.222	1.049	1.048	1.062
Largest difference peak and hole (e Å^{-3})	1.30 and –0.53	0.32 and –0.28	0.25 and –0.31	0.37 and –0.39	0.14 and –0.16	0.68 and –0.36	0.35 and -0.47

Table 5 con't. Crystallographic data for **7**·$2^1/_4$MeCN. **8**, **9**·4toluene, **10**·5MeCN and **11**·1.75toluene·1.25hexane

Compound	**7**·$2^1/_4$MeCN	**8**	**9**·4toluene	**10**·5MeCN	**11**·1.75toluene·1.25hexane
Formula	$C_{59.50}H_{66.75}Al_2N_{6.25}O_2$	$C_{54}H_{58}Al_2N_4O_2$	$C_{108}H_{81}AlCl_4N_8O_8$	$C_{114}H_{116}AlN_{13}O_4$	$C_{264.50}H_{342}Al_{16}N_{16}O_{16}$
Formula weight	955.40	849.00	1787.58	1759.17	4433.20
Crystal system	Triclinic	Triclinic	Triclinic	Monoclinic	Triclinic
Space group	*P*$\bar{1}$	*P*$\bar{1}$	*P*$\bar{1}$	$P2_1/c$	*P*$\bar{1}$
Unit cell dimensions					
a (Å)	15.2938(19)	9.7916(5)	13.8593(10)	16.2328(2)	13.1640(3)
b (Å)	15.671(2)	11.2215(4)	14.7463(10)	27.3761(3)	31.8640(5)
c (Å)	25.086(3)	11.7840(6)	23.7238(17)	23.7006(3)	36.2145(5)
α (º)	93.9493(17)	84.624(4)	95.508(7)	90	113.2940(10)
β (º)	97.1008(16)	66.196(5)	101.879(7)	107.9523(6)	94.715(2)
γ (º)	112.5747(16)	84.347(4)	109.459(7)	90	95.712(2)
V (Å^3)	5464.4(12)	1176.81(10)	4401.9(6)	10019.5(2)	13759.6(4)
Z	4	1	2	4	4
Temperature (K)	150(2)	143(2)	143(2)	120.0(2)	120(2)
Wavelength (Å)	0.6884	0.71073	0.71073	0.71073	0.71073
Calculated density (g.cm^{-3})	1.161	1.198	1.343	1.166	1.072
Absorption coefficient (mm^{-1})	0.100	0.107	0.209	0.080	0.113
Transmission factors (min./max.)	0.987, 0.997	0.906, 1.000	0.514, 1.000	0.973, 0.990	0.564,1.000
Crystal size (mm^3)	0.14 × 0.10 × 0.03	0.80 × 0.50 × 0.40	0.35 × 0.30 × 0.20	0.35 × 0.25 × 0.12	0.80 × 0.50 × 0.40
θ(max) (°)	22.6	26.4	27.4	25.0	29.5
Reflections measured	36298	9795	67195	191662	155744
Unique reflections	15657	4806	20011	17619	64526
R_{int}	0.065	0.023	0.067	0.105	0.051
Reflections with $F^2 > 2\sigma(F^2)$	3428	9183	12308	13161	43448
Number of parameters	1319	283	1054	1095	2792
R_1 [$F^2 > 2\sigma(F^2)$]	0.082	0.047	0.099	0.066	0.085
wR_2 (all data)	0.263	0.127	0.291	0.153	0.255
GOOF, *S*	1.030	1.03	1.021	1.026	1.029
Largest difference peak and hole (e Å^{-3})	0.76 and –0.32	0.45 and –0.35	0.90 and –0.51	0.28 and –0.29	1.44 and –0.59